Modeling a Square Vibrating Plate

by

Linqi Shao

A research paper
presented to the University of Waterloo
in partial fulfillment of the
requirement for the degree of
Master of Mathematics
in
Computational Mathematics

Supervisors:
Prof. Serge D'Alessio,
Prof. Justin Wan

Waterloo, Ontario, Canada, 2018

I hereby declare that I am the sole author of this report. This is a true copy of the report, including any required final revisions, as accepted by my examiners.

I understand that my report may be made electronically available to the public.

Abstract

This report is inspired by the work of Ernst Florens Friedrich Chladni, who visualized the nodal lines on a vibrating plate under resonance. We have investigated two models to reproduce the modes of vibration on a square plate with free edges. Both of the models are solved analytically by separation of variables and numerically using an explicit finite difference method. The first model is based on the wave equation, which produces clear nodal patterns but the patterns are different from the experimental results. However, due to the simplicity of the model, we are able to test different techniques such as the eigenvector/eigenvalue approach, various forcing methods, and beats. The second model is based on elasticity theory which, unlike the wave equation model, involves the mechanical properties of the plate. Though the analytical solution of this model cannot be verified, we applied similar techniques used for the wave equation to estimate the resonant frequencies. The resulting nodal patterns are closer to those observed in the experiments. Related issues and possible future work are also discussed in this report.

Acknowledgements

I would like to thank my supervisors, Dr. Serge D'Alessio and Dr. Justin Wan. Thank you for guiding me and providing countless support in my graduate career.

I would like to thank my parents, Aiyun and Baiqing for always loving me and supporting me whenever I need you.

I would like to thank my second reader, Prof. Sander Rhebergen, for reading and giving me comments to polish this report.

I would like to thank my boyfriend, Xinfu, for providing guidance in making important decisions in my life.

I would like to thank my roomates, Beini and Fan. Thank you for your companionship in past years.

Finally, a big thanks to all my friends in the Computational Mathematics program. Congratulations to everyone!

Dedication

This is dedicated to my family.

Table of Contents

List of Tables

List of Figures

Chapter 1

Introduction

This research is about simulating the motion of a thin square plate using analytical and numerical methods. The thickness of the plate is much smaller than the length of the sides[2]. The aim of the project is to predict the motion of a plate when it is vibrating at a specific frequency.

Figure 1.1: Ernst Chladni.

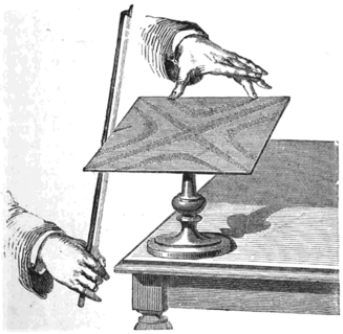

Figure 1.2: Demonstration By Chladni.

The project is motivated by a famous experiment performed by the German physicist and musician, Ernst Florens Friedrich Chladni (Fig. 1.1). He lived from 1756 to 1827, and is called the father of Acoustics because of his work on vibrating plates. His experiments demonstrated how standing waves form on two-dimensional thin plates. The experiments were carried out as follows. The initial set up of the experiment was done using a metallic plate with a fixed centre and a violin bow. To create a constant vibration on the plate, Chladni strummed the violin bow on the side of the plate. Then, to visualize the

displacement of the plate, he sprinkled a layer of powder on to the surface of the plate. The powder was observed to settle along places on the plate which remained stationary, as shown by Fig. 1.2. These patterns are called Chladni patterns [3]. In addition, after numerous experiments, Chladni was able to determine that there is a relationship between the frequency and the patterns for a fixed centre circular plate. These patterns always appear as circles and diameter lines, as shown in Fig. 1.3[4] and Fig. 1.4[5]. Chladni found that $f \sim (m + 2n)^2$ where f is the frequency, m is the number of nodal diameters and n is the number of nodal circles.

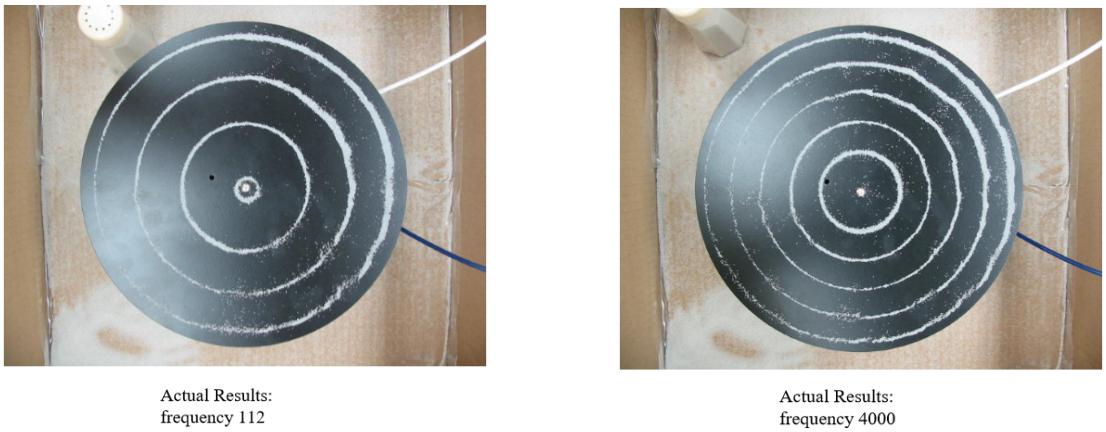

Actual Results:
frequency 112

Actual Results:
frequency 4000

Figure 1.3: Chladni Patterns for a Circular Plate.

Emperor Napoleon helped advance the progress of research on vibrating plates. He was very interested in Chladni's demonstration at the Tuilerie Palace. Thus, in 1809, he commissioned the institut de France to initiate a competition for finding the mathematical theory behind the Chladni patterns. This competition set the foundation for the theory of elasticity. Famous mathematicians, such as Joseph-Louis Lagrange, Pierre-Simon Laplace, Adrien-Marie Legendre, and Simon-Denis Poisson were judges for the competition [6]. Not many mathematicians were interested in the competition, possibly due to the harshness of the judges. Though the competition got off to an unpromising start, the winner of the competition was Sophie Germain, a female French mathematician, shown in Fig. 1.5. During the first launch, the competition had to be extended until it got the first submission, which was from Germain. Unfortunately, she made a mistake in evaluating the strain energy which resulted in an erroneous differential equation. The competition was relaunched in 1813. Again, Germain left out the precise definition of a constant in the equation. Finally, in the third submission in 1816, she won the prize which made her the first woman to receive an award with such importance from institut de France [2]. Though her work was

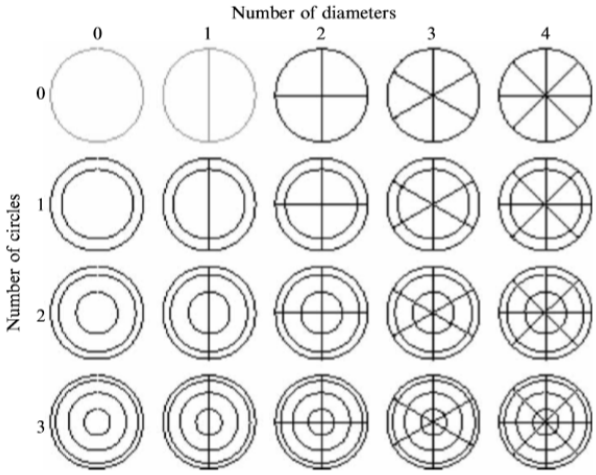

Figure 1.4: Chladni figures for circular plate, sorted by number of diameters and circles in each pattern.

not perfect, she is still honoured for writing the first valid differential equation describing a free vibrating plate[7].

In this essay, we are looking to reproduce the experimental results for a free-edge square plate using numerical and analytical methods. The set up of the experiment is a bit different compared to Chladni's experiment. In order to control the oscillating process better, we used a mechanical wave generator (Fig. 1.6), a uniform square metal plate and sand. The generator is fixed at the centre of the plate and the edges of the plate are free. Thus, when the wave generator is on, the centre of the square plate oscillates at a constant predefined frequency. When the oscillating frequency is equal to a resonance frequency of the plate, the corresponding standing waves would be the major players on the plate. As sand is sprinkled onto the plate, one of the Chladni patterns is visualized. Fig. 1.7 shows five different Chladni patterns observed in the experiment and each of them corresponds to a unique vibrating frequency. The higher the frequency, the more complicated the patterns become. Fig. 1.8 shows some other Chladni figures created in a modern laboratory environment in Munich and San Diego.

In this essay, we use two models to describe the plate motion - a wave equation based model and an elasticity based model. In chapter 2, the physics behind the Chladni patterns based on the wave equation model will be discussed. The wave equation serves as a simpler model to approximate a vibrating plate. Various numerical and analytical results will be presented and compared with experimental observations.

Figure 1.5: Sophie Germain.

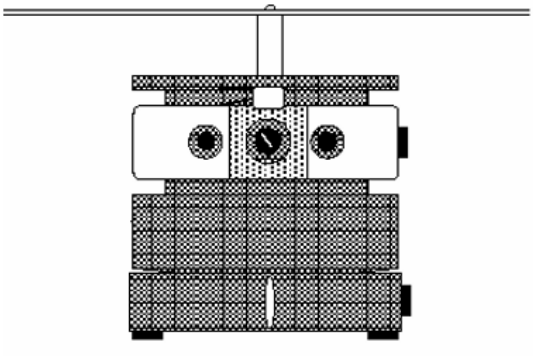

Figure 1.6: A sketch of a wave generator.

In chapter 3, the elasticity based model will be introduced. This model is more realistic compared to the wave equation model. As this model is more complicated than the wave equation model, this chapter will provide more details as to how the equation is solved and how the boundary conditions are enforced. Results and comparisons will also be discussed.

The last chapter will focus on the comparison between the wave equation based model and the elasticity based model. Multiple issues related to numerical methods and analytical solutions will be discussed. Lastly, possible directions of future work will be mentioned as well.

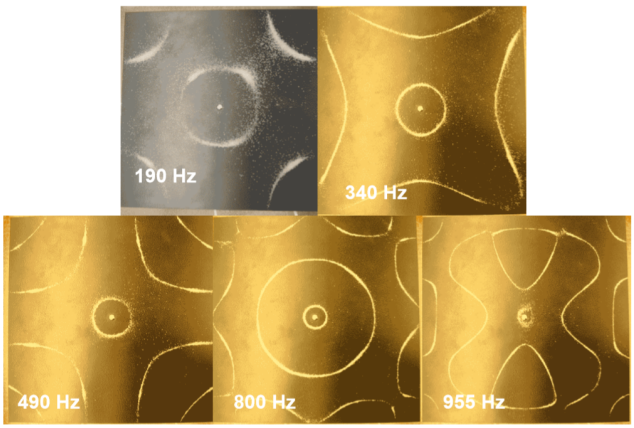

Figure 1.7: Sample Chladni Patterns on Square Plate with Frequencies.

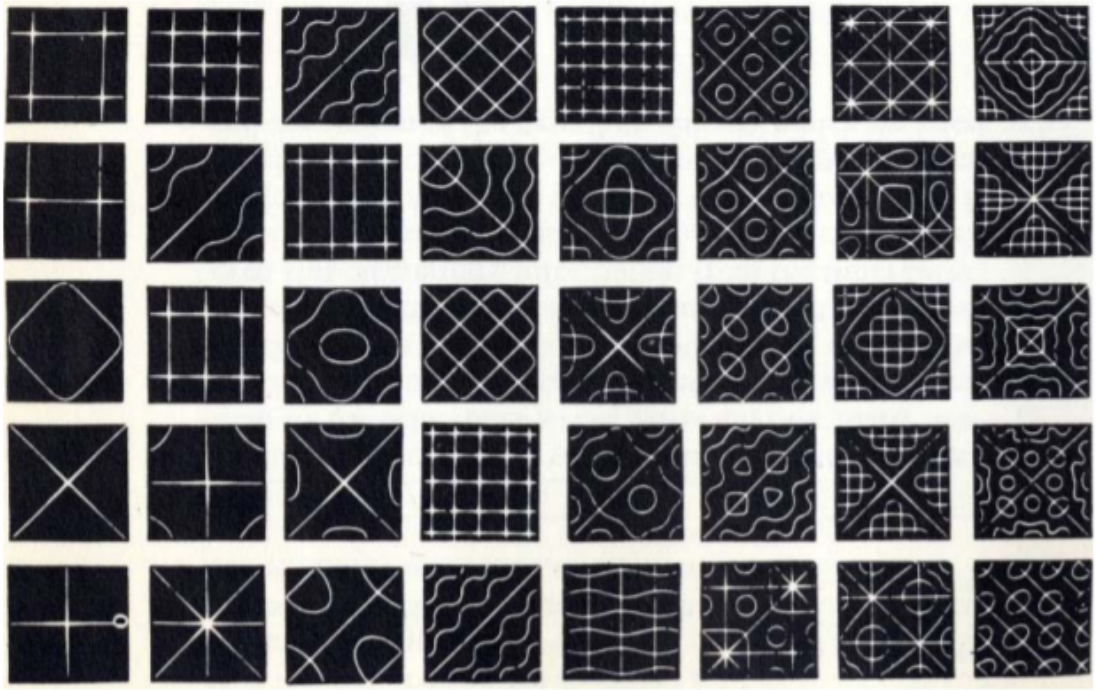

Figure 1.8: Some other Chladni patterns created in a modern laboratory environment[1].

Chapter 2

The Wave Equation Model

Waves, which are often caused by vibrations and disturbances, are one of the most common phenomena in our daily life. With several assumptions, we can approximate the vibrating plate experiment as waves propagating on a thin stretched elastic membrane.

2.1 Introduction to the Wave Equation

The propagation of waves can be described by a hyperbolic partial differential equation, which consists of a time variable, t, and one or more space variables. In our case, we have two spatial variables, x and y. If we let ∇^2 denote the Laplacian operator and c be the propagation speed, the wave equation for u, the displacement of the thin membrane, can be written in the following dimensional form:

$$\frac{\partial^2 u}{\partial t^2} = c^2 \nabla^2 u. \tag{2.1}$$

The derivation and assumptions of the wave equation can be found in [8]. On a square area, ranging from $[-a, a]$, the expanded wave equation is given by:

$$\frac{1}{c^2}\frac{\partial^2 u}{\partial t^2} = \frac{\partial^2 u}{\partial x^2} + \frac{\partial^2 u}{\partial y^2}, -a \leq x, y \leq a. \tag{2.2}$$

Here, the propagation speed c is related to the mass density, ρ, and the tension, τ, through $c^2 = \frac{\tau}{\rho}$.

There are multiple sets of possible spatial boundary conditions for the wave equation. Table 2.1 shows a list of possible boundary conditions with their physical meanings.

The first boundary condition refers to the plate that has fixed edges, which means that there is absolutely no oscillation on the edges of the plate.

The second listed boundary condition stands for the plate that has free edges. A similar situation occurs with a rope having free ends, where the slope at both ends are equal to zero. For each edge on the plate, the gradient in the direction perpendicular to the edge and in the plane of the plate is equal to zero.

The third listed boundary condition refers to the situation when the edges of the plate are moved according to a function f which depends on the spatial variable y and the time variable t.

Type of Support at Edge $x = a$	Mathematical Expressions
Fixed edge	$(u)_{x=a} = 0$
Free-edge	$\left(\frac{\partial u}{\partial x}\right)_{x=a} = 0$
Moving edge	$(u)_{x=a,t=t} = f(y,t)$

Table 2.1: Different types of boundary conditions for wave equation.

Since we want to simulate a free-edge plate with a wave generator producing vibrations, we will work with the second listed boundary condition as follow:

$$\frac{\partial u}{\partial x}(x,y,t) = 0, \text{ along } x = \pm a, \tag{2.3a}$$

$$\frac{\partial u}{\partial y}(x,y,t) = 0, \text{ along } y = \pm a, \tag{2.3b}$$

We will use two sets of initial conditions. The first set of initial conditions corresponds to one of the resonant modes, $U_0(x,y)$, of the plate and with zero initial velocity:

$$u(x,y,0) = U_0(x,y), \tag{2.4a}$$

$$\frac{\partial u}{\partial t}(x,y,0) = 0. \tag{2.4b}$$

The second set of initial conditions is used for simulating the wave equation with an external force term. Here, the plate has zero initial displacement and also zero initial velocity:

$$u(x, y, 0) = 0, \tag{2.5a}$$

$$\frac{\partial u}{\partial t}(x, y, 0) = 0. \tag{2.5b}$$

2.2 Resonance Frequencies and Standing Waves

Sound is caused by the vibration of materials. The higher the frequency, the higher the pitch. When two materials share the same pitch, the listener would hear the sound become either softer or louder. This can be explained by the superposition principal - when two waves meet at one spot, they add together. Constructive interference causes the sound to become louder, which means two waves are in phase, and destructive interference causes the sound to become softer, which means the two waves arrive out of phase[9].

In a similar way, when two waves, with identical frequencies, travel in opposite directions, a standing wave is formed. A standing wave creates constant nodes with zero displacement and anti-nodes with maximum displacement.

It is easy to predict the standing wave in one-dimensional space. For example, on a rope with fixed ends, the standing waves exist whenever the length of the rope is divisible by half of the wavelength, and the corresponding frequency, which is called resonance frequency, can be easily calculated. Indeed, resonance does not only happen with fixed ends. It exits with any boundary conditions but the associated frequency might be different. Therefore, to express the wave pattern in time and space, we can write it as $\cos(\omega t + \gamma)trig(kx)$, where ω is the frequency and γ is the phase constant, $k = \frac{2\pi}{\lambda}$ is the wave number, λ is the wavelength, and $trig$ represents either sine or cosine.

However, things become a bit more complicated in two dimensions. Instead of a stretched string with tension pulling on two ends, we now have an elastic sheet with tension pulling on all edges. In two dimensional space, expressed in a Cartesian coordinate system, the solution that satisfies the wave equation can be written as $\cos(\omega t+\gamma)trig(k_x x)trig(k_y y)$, where k_x and k_y refer to the wave numbers in x and y directions. In the next section, we will discuss the full solution to the two-dimensional wave equation in Cartesian coordinates for a square membrane.

2.3 Solving Wave Equation with Boundary Conditions

The wave equation in two dimensions expressed in Cartesian coordinates is given by equation (2.2). We next want to cast it in dimensionless form.

Let $(x, y) = (a\hat{x}, a\hat{y})$, $t = \frac{a}{c}\hat{t}$ and $u = H\hat{u}$, where H is the displacement amplitude. Then, equation (2.2) can be written as follows:

$$\frac{\partial^2 \hat{u}}{\partial \hat{t}^2} = \frac{\partial^2 \hat{u}}{\partial \hat{x}^2} + \frac{\partial^2 \hat{u}}{\partial \hat{y}^2}, -1 \leq \hat{x}, \hat{y} \leq 1. \tag{2.6}$$

For simplicity of notation, we will write $\hat{u}$, $\hat{x}$, $\hat{y}$, $\hat{t}$ as u, x, y, and t in the rest of this chapter.

By separation of variables, we are able to show that a solution to equation (2.6) is given by:

$$u(x, y, t) = Atrig(k_x x)trig(k_y y)\cos(\omega t + \gamma), \tag{2.7}$$

where A refers to an arbitrary amplitude, ω is the angular frequency, which is related to k_x and k_y through $\omega = \sqrt{k_x^2 + k_y^2}$, and γ is the phase shift.

In order to determine k_x and k_y, we need to apply the boundary conditions. The spatial boundary conditions (2.3) written in dimensionless form are:

$$\frac{\partial u}{\partial x}(x, y, t) = 0, \text{ along } x = \pm 1, \tag{2.8a}$$

$$\frac{\partial u}{\partial y}(x, y, t) = 0, \text{ along } y = \pm 1. \tag{2.8b}$$

The initial conditions (2.4) written in dimensionless form are:

$$u(x, y, 0) = U_0(x, y), \tag{2.9a}$$

$$\frac{\partial u}{\partial t}(x, y, 0) = 0. \tag{2.9b}$$

Applying the free-edge boundary conditions, a solution for a free edge square plate is $u(x, y, t) = A_{ms}\cos(m\pi x)\cos(s\pi y)\cos(\omega t)$, where m and s are integers identifying a

specific mode, and $\omega = \pi\sqrt{m^2 + s^2}$. The most general solution for $u(x, y, t)$ is the sum of these modes:

$$u(x, y, t) = \sum_{m,s=1}^{\infty} A_{ms} \cos(\omega_{ms} t) \cos(m\pi x) \cos(s\pi y) . \tag{2.10}$$

The constant A_{ms} can be obtained by applying the initial condition from equation (2.9):

$$A_{ms} = \int_{-1}^{1} \int_{-1}^{1} U_0(x, y) \cos(m\pi x) \cos(s\pi y)\, dxdy. \tag{2.11}$$

Now, how do we find the Chladni patterns? Note that for a specific frequency ω, there are one or more distinct vibrations sharing the same frequency. When $\omega = \sqrt{2}\pi$, there is only one possibility for m and s, which is $\{m = s = 1\}$. This is the case when there is only one mode of vibration. When $\omega = \sqrt{50}\pi$, there are three possibilities for m and s, which are $\{m = s = 5\}$, $\{m, s = 1, 7\}$ and $\{m, s = 7, 1\}$. This is the case when there are three modes of vibration. In this essay, we are only going to discuss the interesting base case - $\omega = \sqrt{5}\pi$.

Now, for the frequency $\omega = \pi\sqrt{1^2 + 2^2} = \sqrt{5}\pi$, there are two modes of vibration having the same frequency:

$$\cos(\pi x) \cos(2\pi y) \text{ and } \cos(2\pi x) \cos(\pi y). \tag{2.12}$$

In the wave equation model, when the membrane vibrates at frequency $\sqrt{5}\pi$, it would be naturally vibrating with the combination of the two modes mentioned above. Therefore, the general spatial form of the plate deflection will be of the form:

$$C \cos(\pi x) \cos(2\pi y) + D \cos(2\pi x) \cos(\pi y), \tag{2.13}$$

where C and D are arbitrary constants. With given C, D , m, and s, the nodal lines, or the Chladni patterns, satisfy the following equation:

$$C \cos(m\pi x) \cos(s\pi y) + D \cos(s\pi x) \cos(m\pi y) = 0. \tag{2.14}$$

By symmetry, we can set $C = D = 1$. With $(m, s) = (1, 2)$ or $(2, 1)$, the theoretical nodal pattern is shown in Fig. 2.1. By comparison with the experimental results, the closest Chladni pattern observed is shown in Fig. 1.7 and corresponds to a frequency $\omega = 190Hz$. We see that the theoretical nodal pattern yields an extra square shape. This may be caused by the simple and inadequate wave equation model.

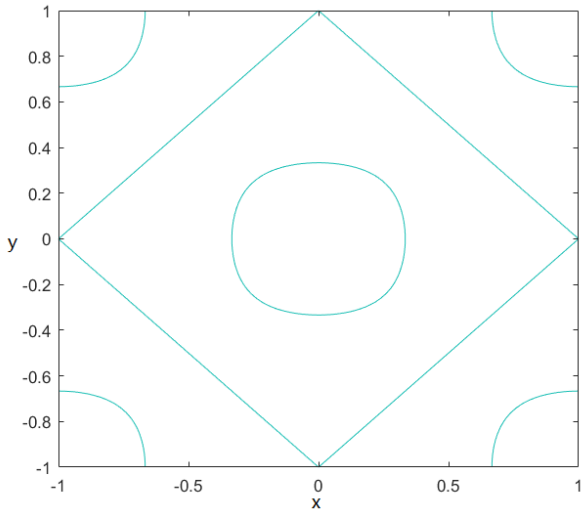

Figure 2.1: Nodal lines for the (1,2), (2,1) modes.

2.4 The Damped Wave Equation

In the real world, friction is always present. We can account for this by adding a damping term to the wave equation. For the freely vibrating plate, a major source of friction is air, which has a magnitude proportional to the speed of the plate movement but in the opposite direction. Therefore, the term has the form $-\beta\frac{\partial u}{\partial t}$ where β denotes the dimensionless damping coefficient. The wave equation then becomes:

$$\frac{\partial^2 u}{\partial t^2} = \frac{\partial^2 u}{\partial x^2} + \frac{\partial^2 u}{\partial y^2} - \beta\frac{\partial u}{\partial t}, \quad -1 \leq x, y \leq 1, t \geq 0. \tag{2.15}$$

We can solve this equation using separation of variables by setting $u(x, y, t) = X(x)Y(y)T(t)$. Equation (2.15) becomes:

$$\frac{\frac{d^2T}{dt^2} + \beta\frac{dT}{dt}}{T} = \frac{\frac{d^2X}{dx^2}}{X} + \frac{\frac{d^2Y}{dy^2}}{Y} = -k^2. \tag{2.16}$$

As before, $k^2 = m^2\pi^2 + s^2\pi^2$ where m, s are integers. Next, solving the ordinary differential equation $T'' + \beta T' + \pi^2(m^2 + s^2)T = 0$ yields:

$$T(t) = e^{-\frac{\beta}{2}t}[A\cos(\omega t) + B\sin(\omega t)],$$

where $\omega = \pi\sqrt{(m^2+s^2) - \frac{\beta^2}{4\pi^2}}$. As $\beta \to 0$, $\omega \to \pi\sqrt{m^2+s^2}$ which is equivalent to the undamped frequency, as expected.

Thus, for a damped vibrating plate with free edges, the general solution is given by:

$$u(x,y,t) = \sum_{m,s=1}^{\infty} e^{-\frac{\beta}{2}t}[A_{ms}\cos(\omega t) + B_{ms}\sin(\omega t)]\cos(m\pi x)\cos(s\pi y). \tag{2.17}$$

If we impose the initial conditions:

$$u(x,y,0) = U_0(x,y), \tag{2.18a}$$

$$\frac{\partial u}{\partial t}(x,y,0) = 0, \tag{2.18b}$$

then $B_{ms} = \frac{\beta}{2\omega}A_{ms}$ and A_{ms} is given by equation (2.11).

2.5 Numerical Solution Procedure

In this section we will discuss how to discretize the wave equation model so that we can solve it numerically. Since the only influence from the damping term is to continuously reduce the amplitude of the plate displacement, and it does not influence the shape of nodal patterns, we will set $\beta = 0$ and solve the undamped wave equation model numerically using the finite difference method.

First, we will show how to approximate each term in the wave equation using finite difference expressions. We use the notation $u_{i,j}^k$ to represent the numerical approximation to $u(x_i, y_j, t_k)$ where the mesh points (x_i, y_j, t_k) are defined by:

$$x_i = -1 + i\Delta x, y_j = -1 + j\Delta y, t_k = k\Delta t,$$

where i, j and k are non-negative integers. Here, Δx is the uniform grid spacing in the x direction, Δy is the uniform grid spacing in the y direction, and Δt is the uniform time step. Let $h = \Delta x = \Delta y$, then the limits for i and j are $i \leq \frac{2}{h}$, and $j \leq \frac{2}{h}$. If we let the stopping time be T, then $k \leq \frac{T}{\Delta t}$.

Below are centered-difference approximations for the following derivatives:

$$\frac{\partial^2 u}{\partial t^2}(x_i, y_j, t_k) \approx \frac{u_{i,j}^{k-1} - 2u_{i,j}^k + u_{i,j}^{k+1}}{(\Delta t)^2}, \tag{2.19a}$$

$$\frac{\partial^2 u}{\partial x^2}(x_i, y_j, t_k) \approx \frac{u_{i-1,j}^k - 2u_{i,j}^k + u_{i+1,j}^k}{h^2}, \tag{2.19b}$$

$$\frac{\partial^2 u}{\partial y^2}(x_i, y_j, t_k) \approx \frac{u_{i,j-1}^k - 2u_{i,j}^k + u_{i,j+1}^k}{h^2}. \tag{2.19c}$$

If we assume that $u_{i,j}^k$ for all possible values of i, j and k are exact, the local truncation error, $\tau_{i,j}^k$, at mesh point (x_i, y_j, t_k), satisfies the following equation:

$$\frac{u_{i,j}^{k-1} - 2u_{i,j}^k + u_{i,j}^{k+1}}{(\Delta t)^2} = \frac{u_{i-1,j}^k - 2u_{i,j}^k + u_{i+1,j}^k}{h^2} + \frac{u_{i,j-1}^k - 2u_{i,j}^k + u_{i,j+1}^k}{h^2} + \tau_{i,j}^k. \tag{2.20}$$

Since $\frac{\partial^2 u}{\partial t^2} = \frac{\partial^2 u}{\partial x^2} + \frac{\partial^2 u}{\partial y^2}$, the above equation can be written as:

$$\begin{aligned} \frac{u_{i,j}^{k-1} - 2u_{i,j}^k + u_{i,j}^{k+1}}{(\Delta t)^2} - \frac{\partial^2 u}{\partial t^2}(x_i, y_j, t_k) =& \frac{u_{i-1,j}^k - 2u_{i,j}^k + u_{i+1,j}^k}{h^2} - \frac{\partial^2 u}{\partial x^2}(x_i, y_j, t_k) \\ &+ \frac{u_{i,j-1}^k - 2u_{i,j}^k + u_{i,j+1}^k}{h^2} - \frac{\partial^2 u}{\partial y^2}(x_i, y_j, t_k) \\ &+ \tau_{i,j}^k. \end{aligned} \tag{2.21}$$

By the Taylor expansion we know that:

$$\frac{u_{i,j}^{k-1} - 2u_{i,j}^k + u_{i,j}^{k+1}}{(\Delta t)^2} - \frac{\partial^2 u}{\partial t^2}(x_i, y_j, t_k) = \frac{(\Delta t)^2}{12}\frac{\partial^4 u}{\partial t^4}(x_i, y_j, t_k) + O((\Delta t)^4), \tag{2.22a}$$

$$\frac{u_{i-1,j}^k - 2u_{i,j}^k + u_{i+1,j}^k}{(\Delta x)^2} - \frac{\partial^2 u}{\partial x^2}(x_i, y_j, t_k) = \frac{h^2}{12}\frac{\partial^4 u}{\partial x^4}(x_i, y_j, t_k) + O(h^4), \tag{2.22b}$$

$$\frac{u_{i,j-1}^k - 2u_{i,j}^k + u_{i,j+1}^k}{(\Delta y)^2} - \frac{\partial^2 u}{\partial y^2}(x_i, y_j, t_k) = \frac{h^2}{12}\frac{\partial^4 u}{\partial y^4}(x_i, y_j, t_k) + O(h^4), \tag{2.22c}$$

The local truncation error $\tau_{i,j}^k$, is then equal to:

$$\tau_{i,j}^k = \frac{(\Delta t)^2}{12}\frac{\partial^4 u}{\partial t^4}(x_i, y_j, \kappa_k) - \frac{h^2}{12}\frac{\partial^4 u}{\partial x^4}(\xi_i, y_j, t_k) - \frac{h^2}{12}\frac{\partial^4 u}{\partial y^4}(x_i, \varrho_j, t_k), \tag{2.23}$$

where $\kappa_k \in (t_{k-1}, t_{k+1})$, $\xi_i \in (x_{i-1}, x_{i+1})$ and $\varrho_j \in (y_{j-1}, y_{j+1})$.

The above finite difference method yields a recurrence relation. If we exclude the local truncation error and solve for $u_{i,j}^{k+1}$, we obtain the explicit difference equation:

$$u_{i,j}^{k+1} = 2u_{i,j}^{k} - u_{i,j}^{k-1} + \frac{(\Delta t)^2}{h^2}\left(u_{i-1,j}^{k} - 2u_{i,j}^{k} + u_{i+1,j}^{k}\right) + \frac{(\Delta t)^2}{h^2}\left(u_{i,j-1}^{k} - 2u_{i,j}^{k} + u_{i,j+1}^{k}\right). \quad (2.24)$$

The next step is to deal with the boundary conditions given by equation (2.8). We are going to use the central difference method to approximate the first-order derivatives. Take $\frac{\partial u}{\partial x}(x_i, y_j, t_k)$ as an example, below are the central difference approximations and the associated local truncation error $\hat{\tau}$, assuming that numerical approximations are exact, for the first-order derivatives:

$$\frac{\partial u}{\partial x}(x_i, y_j, t_k) \approx \frac{u_{i+1,j}^{k} - u_{i-1,j}^{k}}{2h}, \quad (2.25a)$$

$$\hat{\tau} = \frac{u_{i+1,j}^{k} - u_{i-1,j}^{k}}{2h} - \frac{\partial u}{\partial x}(x_i, y_j, t_k) = \frac{h^2}{6}\frac{\partial^3 u}{\partial x^3}(x_i, y_j, t_k) + O(h^4). \quad (2.25b)$$

By applying this difference scheme along the edges with boundary conditions (2.8), we have approximations for the ghost points as below:

$$u_{n+1,j} = u_{n-1,j}, \quad (2.26a)$$

$$u_{-1,j} = u_{1,j}, \quad (2.26b)$$

$$u_{i,n+1} = u_{i,n-1}, \quad (2.26c)$$

$$u_{i,-1} = u_{i,1}. \quad (2.26d)$$

For the time step size, Δt, we have to set a restriction so that the numerical scheme is stable. By applying the Fourier method, we can show that the explicit scheme is stable if and only if $\Delta t \leq \frac{h}{\sqrt{2}}$ [10].

Implementing the Numerical Method

Here, we consider an example with initial conditions given by equation (2.9), where the initial displacement, $U_0(x, y)$, corresponds to standing waves at frequency $\omega = \sqrt{5}\pi$:

$$U_0(x, y) = \cos(\pi x)\cos(2\pi y) + \cos(2\pi x)\cos(\pi y). \quad (2.27)$$

In addition, as $\frac{\partial u}{\partial t}(x, y, 0) = 0$, we can approximate the plate displacement to be $U_0(x, y)$ both near and at $t = 0$.

Next, we let $h = 0.02$ and based on the stability requirement, we choose $\Delta t = \frac{h}{2} = 0.01$. The grid is then $(n+1) \times (n+1)$ where $n = \frac{2}{h} = 100$. The sample code is given in appendix A.1.

In theory, the nodal lines of the resulting solution should remain constant over time as the initial displacement is set to be a combination of standing waves. When the dimensionless time reaches 10, the resulting displacement of the plate and the corresponding nodal lines are shown in Fig. 2.2. Note that at $t = 0$, the nodal pattern is the theoretical nodal pattern shown in Fig. 2.1. If we compare the two nodal patterns, we can see that the two patterns look the same. Indeed, within the time range from 0 to 10, the shape of the nodal pattern never changes. This agrees with the theory, that when the initial displacement is set to be some standing waves, the nodal pattern remains the same over time.

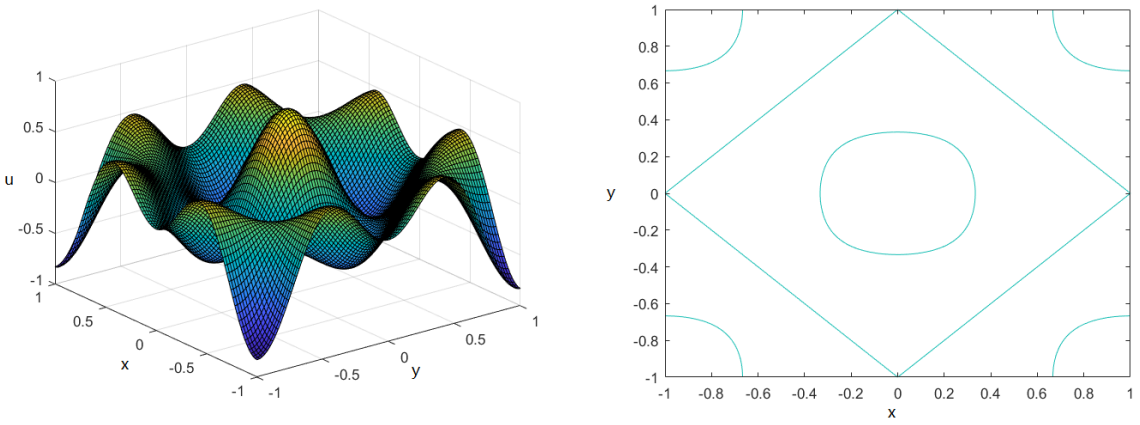

Figure 2.2: Plate displacement and the corresponding nodal lines at time $T = 10$.

2.6 Forced Wave Equation

In the previous section, we assumed that the plate has an initial displacement equivalent to standing waves associated with frequency $\omega = \sqrt{5}\pi$ and let it vibrate freely. We verified that the nodal lines corresponding to the standing waves remain fixed on the plate for a relatively long time when the difference scheme in equation (2.19) is applied. However, that simulation is very different from the experiment we conducted.

In the physical experiment, the plate starts at rest with zero displacement, and a periodic external force is applied at the centre of the plate. If the external force has frequency equal to one of the resonance frequencies, then over time the corresponding standing waves should dominate the plate. For example, if the external force has a frequency $\sqrt{5}\pi$, the dominating pattern should be the same as that shown in Fig. 2.1 after some time.

How should we add the force term to the undamped wave equation? With the force term the wave equation becomes:

$$\frac{\partial^2 u}{\partial t^2}(x,y,t) = \frac{\partial^2 u}{\partial x^2}(x,y,t) + \frac{\partial^2 u}{\partial y^2}(x,y,t) + Q(x,y,t), \tag{2.28}$$

where $Q(x,y,t)$ represents a time and spatially dependent external force term [11].

To match the experiment, we apply the following initial conditions:

$$u(x,y,0) = 0, \tag{2.29a}$$

$$\frac{\partial u}{\partial t}(x,y,0) = 0, \tag{2.29b}$$

which correspond to zero initial displacement and zero initial velocity.

Suppose that the external force has a frequency $\omega = \sqrt{5}\pi$, then $Q(x,y,t)$ has a periodic form, $Q_0(x,y)\cos(\omega t)$. Since the wave generator applies the force to the centre of the plate, we consider the spatial force term $Q_0(x,y)$ to be:

$$Q_0(x,y) = \begin{cases} \alpha, & \text{if } x = y = 0 \\ 0, & \text{otherwise} \end{cases}, \tag{2.30}$$

where α denotes the strength.

At resonance, the oscillation of modes corresponding to the forcing frequency should grow in time without bound [11]. Thus, theoretically, we should observe the amplitude of the displacement of the plate to increase with time and the nodal lines should approach the pattern shown in Fig. 2.1.

Numerically Solving the Forced Wave Equation

We use the basic set up for the Cartesian grid as in the previous example, where $h = 0.02$, and $\Delta t = 0.01$. However, the plate has initial displacement $u(x,y,0) = 0$. The force

strength was set to $\alpha = 5$, and frequency $\omega = \sqrt{5}\pi$. Thus, the force term is given by:

$$Q(x, y, t) = \begin{cases} 5\cos(\sqrt{5}\pi t), & \text{if } x = y = 0 \\ 0, & \text{otherwise} \end{cases}. \tag{2.31}$$

The explicit finite difference equation becomes:

$$\begin{aligned} u_{i,j}^{k+1} &= 2u_{i,j}^{k} - u_{i,j}^{k-1} \\ &+ \frac{(\Delta t)^2}{h^2}(u_{i-1,j}^{k} - 4u_{i,j}^{k} + u_{i+1,j}^{k} + u_{i,j-1}^{k} - 2u_{i,j}^{k} + u_{i,j+1}^{k}) + (\Delta t)^2 Q(x_i, y_j, t_k). \end{aligned} \tag{2.32}$$

The code is given in appendix A.2. As the plate started with zero initial displacement, it takes longer for it to reach a relatively stable nodal pattern. As time passes, the shape of the nodal lines gets closer to the theoretical nodal pattern. Fig. 2.3 shows the change of shapes of the nodal patterns starting from $t = 5$ to $t = 100$. While the shape of the nodal pattern gets closer to the theoretical pattern, the amplitudes of the oscillations at non-nodal points are also increased. When the dimensionless time reaches 100, the resulting displacement of the plate and the corresponding nodal lines are shown in Fig. 2.4. As expected, the nodal pattern agrees with the shape shown in Fig. 2.1.

2.7 Results and Discussions

Error Analysis

In this section we present some additional results. We begin by discussing the errors in the numerical solution. As mentioned in the previous sections, the local truncation error in this discretization scheme is second order. Thus, theoretically, as we reduce h by a factor of 2, the local error, L^2 *norm* of the difference between the computed and exact solution, should be reduced roughly by $\frac{1}{4}$. For a fixed number of time steps, T, and a fixed ratio $\frac{h}{\Delta t} = 2$, the local error accumulates over a number of time steps $t_n = \frac{T}{\Delta t} = \frac{2T}{h}$, and we should observe that the global error is reduced roughly by $\frac{1}{2}$ when h is reduced by half.

Here is how the error was computed. Since we have the analytical solution to the wave equation, $\cos(\omega t)(\cos(mx)\cos(sy) + \cos(sx)\cos(my))$, we are able to compute the difference between the numerical solution and the analytical solution at any time T. The difference at each mesh point are stored in a vector. The error is computed based on the Euclidean norm of the vector. Let d_i be the difference between the numerical solution and

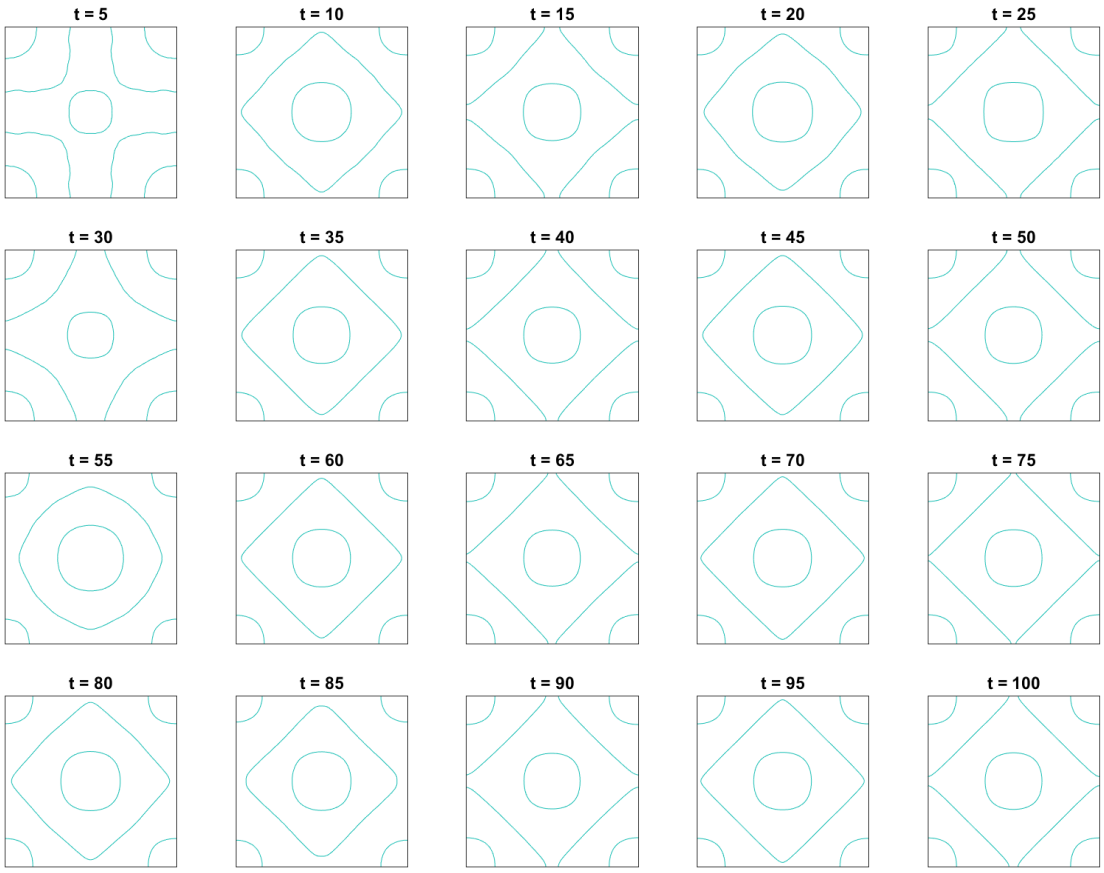

Figure 2.3: The forced wave equation model with forcing frequency $\omega = \pi\sqrt{5}$.

the exact solution at each mesh point i, and N be the total number of mesh points, then the Euclidean norm of the vector is computed as:

$$Euclidean\ Norm = \sqrt{\sum_{i=1}^{N} d_i^2}. \tag{2.33}$$

Note that equation (2.33) is only computed for the norm of the vector, and what we want is the L^2 *norm* of the function. Thus, we need to use the Riemann sum approximation:

$$||u - u_{exact}||_2^2 = \int_{-1}^{1}\int_{-1}^{1}(u - u_{exact})^2 dxdy \approx h^2 \sum_{i=0}^{n}\sum_{j=0}^{n} ||u_{i,j} - u_{exact}(x_i, y_j)||^2, \tag{2.34}$$

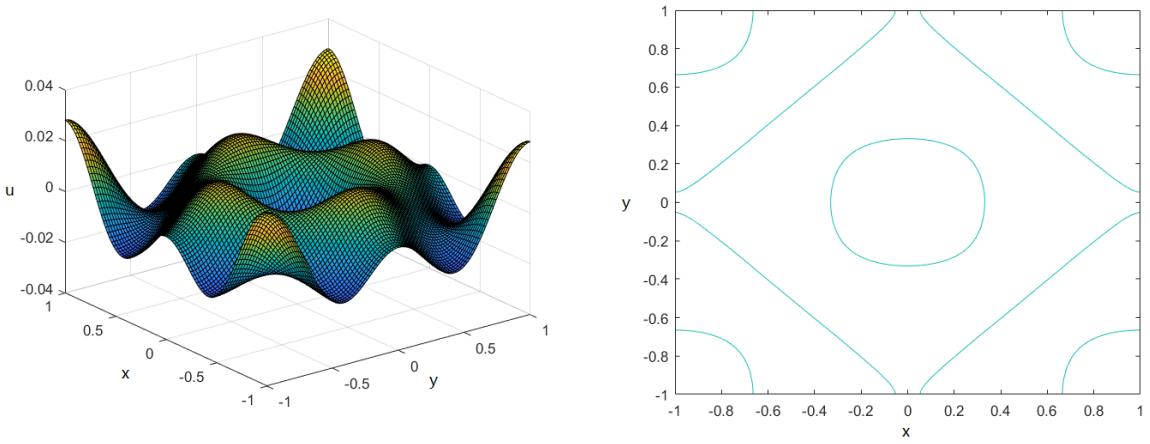

Figure 2.4: Plate displacement and the corresponding nodal lines at time $T = 100$.

where u is the numerical solution to the wave equation at time T, and u_{exact} is the analytical solution to the wave equation at time T. We know that:

$$\sum_{i=1}^{N} d_i^2 \equiv \sum_{i=0}^{n} \sum_{j=0}^{n} ||u_{i,j} - u_{exact}(x_i, y_j)||^2, \tag{2.35}$$

The error is computed as:

$$||u - u_{exact}||_2 \approx h \sqrt{\sum_{i=1}^{N} d_i^2} = h \times Euclidean\ Norm. \tag{2.36}$$

If we let time $T = 1$, the corresponding errors and the ratios between consecutive errors are shown in Table 2.2. Within the table, we can see that the ratio of errors converges to 2 which confirms the hypothesis that as h is reduced by one half, the error should also be reduced by one half. The relationship between errors and the size of h is shown in Fig. 2.5.

Eigenvalue/Eigenvector Approach

Next, we discuss an alternate method for computing the nodal patterns - the eigenvalue/eigenvector method. When we were solving for $u(x, y, t)$ based on the wave equation,

Length of h	Error	Ratio
0.1	0.10878	-
0.05	0.07121	1.5276
0.025	0.03903	1.8246
0.0125	0.02027	1.9250
0.00625	0.01032	1.9655
0.003125	0.00520	1.9834

Table 2.2: The errors and the ratio between errors.

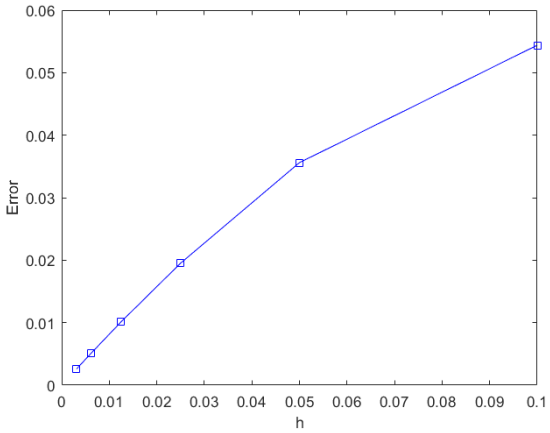

Figure 2.5: Error vs grid size h.

we assumed that time and space were separable, which implies $u(x, y, t) = T(t)F(x, y)$. Thus, based on the wave equation, we have:

$$F\frac{d^2T}{dt^2} = T\left(\frac{\partial^2 F}{\partial x^2} + \frac{\partial^2 F}{\partial y^2}\right). \tag{2.37}$$

If we assume that $T(t) = \cos(\omega t)$, then the wave equation becomes:

$$F\frac{d^2T}{dt^2} = -\omega^2 TF = T(\frac{\partial^2 F}{\partial x^2} + \frac{\partial^2 F}{\partial y^2}), \tag{2.38}$$

where ω refers to the vibrating frequency. Next, by letting $\lambda = -\omega^2$, $D \equiv \frac{\partial^2}{\partial x^2} + \frac{\partial^2}{\partial y^2}$, and dividing equation (2.38) by the common term T, we end up with the equation:

$$DF = \lambda F. \tag{2.39}$$

If we expresss F as the following vector which contains all the values of the displacement $u(x_i, y_j)$ at the mesh points of the plate:

$$F = \begin{pmatrix} f_{0,0} \\ \vdots \\ f_{i,j} \\ f_{i,j+1} \\ \vdots \\ f_{i+1,j} \\ f_{i+1,j+1} \\ \vdots \\ f_{n,n} \end{pmatrix},$$

then based on the numerical discretization given by equation (2.19), for each mesh point on the plate, $f_{i,j} \equiv F(x_i, y_j)$, we obtain:

$$\lambda f_{i,j} = \frac{1}{h^2}(f_{i+1,j} + f_{i-1,j} + f_{i,j+1} + f_{i,j-1} - 4f_{i,j}) + O(h^2),\ i, j = 0, \ldots, n. \tag{2.40}$$

The operator D could be approximated by a matrix M, where M is a large block tridiagonal matrix, of size $(n+1)^2 \times (n+1)^2$, having the form:

$$M = \frac{1}{h^2}\begin{pmatrix} B_1 & I & 0 & \ldots & \ldots & \ldots & \ldots & \ldots & 0 \\ I & B & I & \ddots & & & & & \vdots \\ 0 & I & B & I & \ddots & & & & \vdots \\ \vdots & \ddots & \ddots & \ddots & \ddots & \ddots & & & \vdots \\ \vdots & & \ddots & \ddots & \ddots & \ddots & \ddots & & \vdots \\ \vdots & & & \ddots & \ddots & \ddots & \ddots & \ddots & \vdots \\ \vdots & & & & 0 & I & B & I & 0 \\ \vdots & & & & & 0 & I & B & I \\ 0 & \ldots & \ldots & \ldots & \ldots & \ldots & 0 & I & B_1 \end{pmatrix},$$

where B_1 and B are $(n+1)\times(n+1)$ sparse matrices. The diagonal entries record coefficients in front of $u^k_{i,j}$ and other non-zero entries record coefficients in front of either $u^k_{i,j-1}$ or $u^k_{i,j+1}$ for arbitrary i's, j's and k's. B_1 includes the coefficients in front of mesh points on the

corners and edges, and B includes the coefficients in front of mesh points on the edges and inside. B_1 and B are as follows:

$$B_1 = \begin{pmatrix} -2 & 1 & 0 & \dots & \dots & \dots & \dots & \dots & 0 \\ 1 & -3 & 1 & \ddots & & & & & \vdots \\ 0 & 1 & -3 & 1 & \ddots & & & & \vdots \\ \vdots & \ddots & \ddots & \ddots & \ddots & \ddots & & & \vdots \\ \vdots & & \ddots & \ddots & \ddots & \ddots & \ddots & & \vdots \\ \vdots & & & \ddots & \ddots & \ddots & \ddots & \ddots & \vdots \\ \vdots & & & & 0 & 1 & -3 & 1 & 0 \\ \vdots & & & & & 0 & 1 & -3 & 1 \\ 0 & \dots & \dots & \dots & \dots & \dots & 0 & 1 & -2 \end{pmatrix},$$

$$B = \begin{pmatrix} -3 & 1 & 0 & \dots & \dots & \dots & \dots & \dots & 0 \\ 1 & -4 & 1 & \ddots & & & & & \vdots \\ 0 & 1 & -4 & 1 & \ddots & & & & \vdots \\ \vdots & \ddots & \ddots & \ddots & \ddots & \ddots & & & \vdots \\ \vdots & & \ddots & \ddots & \ddots & \ddots & \ddots & & \vdots \\ \vdots & & & \ddots & \ddots & \ddots & \ddots & \ddots & \vdots \\ \vdots & & & & 0 & 1 & -4 & 1 & 0 \\ \vdots & & & & & 0 & 1 & -4 & 1 \\ 0 & \dots & \dots & \dots & \dots & \dots & 0 & 1 & -3 \end{pmatrix},$$

and I is the identity matrix recording the coefficients in front of either $u^k_{i-1,j}$ or $u^k_{i+1,j}$, with size $(n+1) \times (n+1)$.

As a result, we can rewrite equation (2.39) to $O(h^2)$ as:

$$MF = \lambda F. \tag{2.41}$$

Equation (2.41) becomes an eigenvalue/eigenvector problem for matrix M. We can numerically solve for its eigenvalues and eigenvectors. Table 2.3 lists the first 10 largest eigenvalues with $h = 0.02$. In this table, we see that there are pairs of identical eigenvalues. This can be explained by the fact that each resonance frequency is able to excite more than

λ
1.14589×10^{-13}
-2.41858
-2.41858
-4.83717
-9.67201
-9.67201
-12.09060
-12.09060
-19.34402
-21.75326

Table 2.3: The 10 largest eigenvalues.

one linearly independent mode. The eigenvectors can be interpreted as standing waves on the plate.

Since $\lambda = -\omega^2$, there are many eigenvalues which have their absolute values approximately equal to the square of resonance frequencies given by $\omega = \pi\sqrt{m^2 + s^2}$. For example, there exists a pair of eigenvalues equal to -48.3227 and $-(\sqrt{5}\pi)^2 \approx -49.3480$. Fig. 2.6 shows the nodal patterns of the two linearly independent eigenvectors associated with eigenvalue -48.3227.

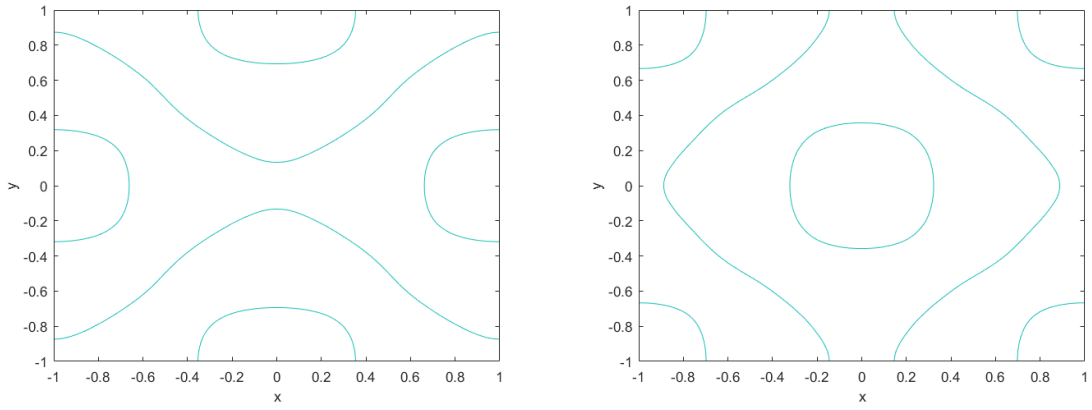

Figure 2.6: The nodal lines for the two eigenvectors associated with eigenvalue -48.3227.

Although the nodal pattern shown in right-hand-side of Fig. 2.6 looks similar to the theoretical pattern shown in Fig. 2.1, the one on the left in Fig. 2.6 does not. The nodal

pattern should be a linear combination of these two independent patterns; however, there is no intuitive way to compute the coefficients in front of the linear combination. If we simply add the two nodal patterns together, it results in a pattern that does not agree closely with the theoretical one.

Interestingly, to plot the nodal patterns for an eigenvector, we need to map the vector into a matrix. Based on the symmetry of the plate, we know that the transpose of the resulting matrix also has to be a standing wave, and it has to be a linear combination of all the eigenvectors associated with the same eigenvalue. Still taking the eigenvalue -48.3227 as an example, we let the two associated eigenvectors be V_1 and V_2, and their mapped matrices be M_1 and M_2. We discovered that the nodal patterns for the sum of M_1 and its transpose M_1^T, and the sum of M_2 and its transpose M_2^T, are both very similar to the theoretical nodal pattern. Figure 2.7 shows the nodal patterns that result in the sum of the eigenvetors and their transposes. That is, the nodal pattern of $M_1 + M_1^T$ is very similar to the nodal pattern of $M_2 + M_2^T$. We also observed this to be true for all the eigenvectors sharing the same eigenvalues.

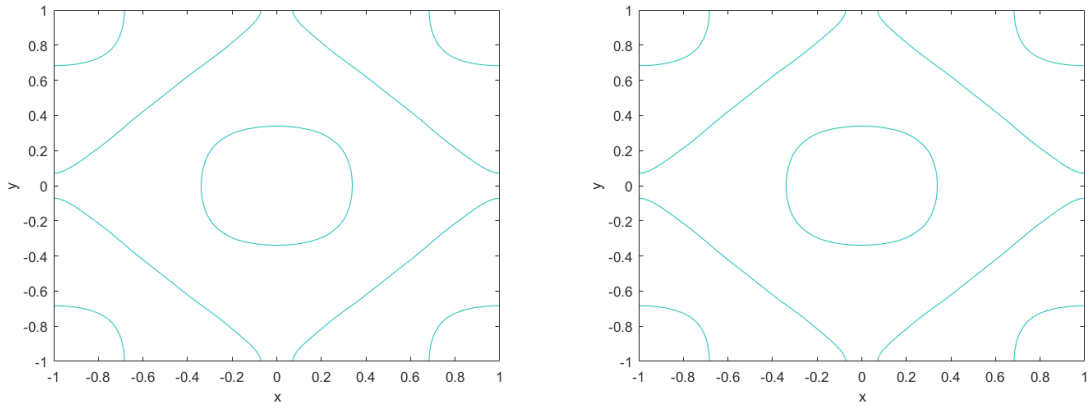

Figure 2.7: The nodal lines for sums of eigenvectors and their transposes associated with eigenvalue -48.3227.

From Table 2.3, we could see that there are many eigenvalues that are not associated with any theoretical resonance frequency. This is because we selected standing waves which have a non-zero displacement at the centre of the plate. Other eigenvalues will have nodal patterns with zero displacement at the centre of the plate. Figure 2.8 shows some of these other nodal patterns.

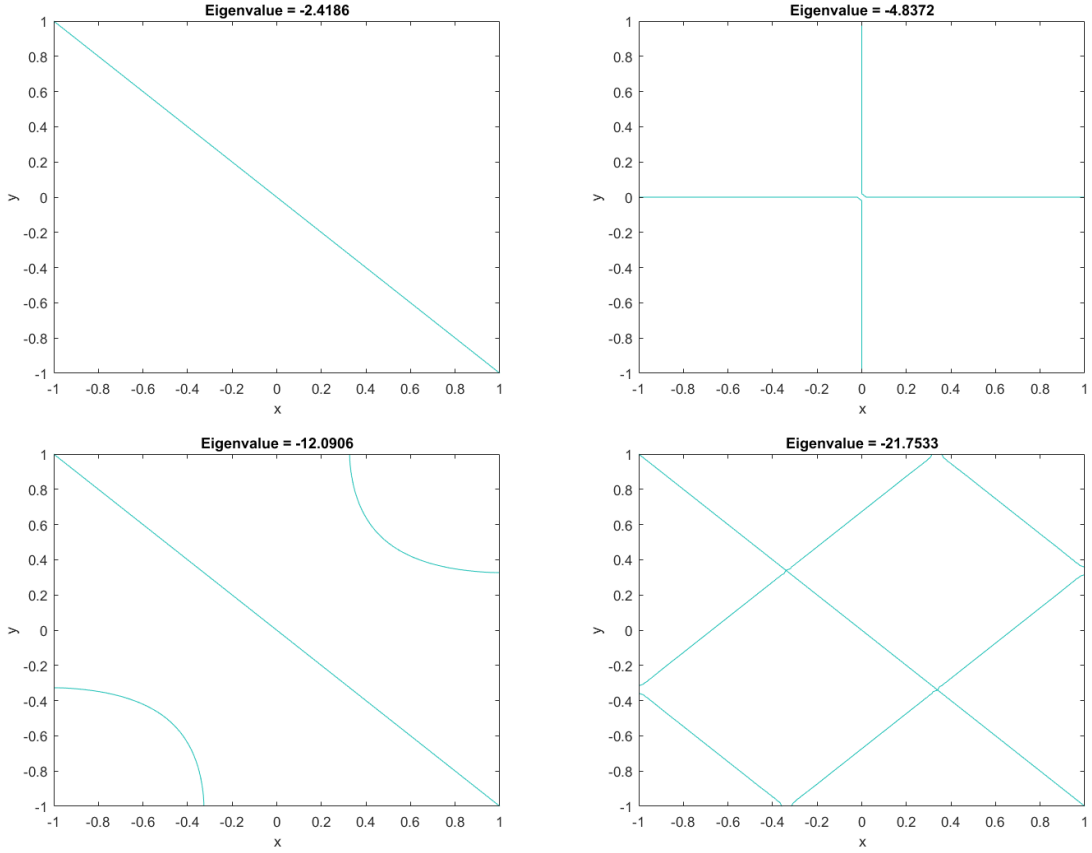

Figure 2.8: Some nodal patterns that are not associated with the theoretical resonance frequencies.

Beats Effect Observed in Forced Wave Equation

In the forced wave equation, we forced the plate at a frequency $\sqrt{5}\pi$, and observed how the displacement at non-nodal points changed over time. In theory, if we are forcing the plate at the resonance frequency, we should observe the amplitudes to become infinite as time goes to infinity. However, when we ran the program for a long time, we observed that the amplitudes of displacements of non-nodal points behaved differently. The phenomenon we observed could be explained by beats [12].

In particular, we will discuss the displacement of the corner $(x, y) = (1, 1)$ of the plate with time as shown in Fig. 2.9 and Fig. 2.10 using $h = 0.02$ and $t = 0.01$. These plots illustrate a beat pattern appearing. Beats form when the forcing frequency ω is close to a

resonance frequency, ω_0, of the plate and can be described mathematically as [13]:

$$BeatPattern = \sin[\frac{1}{2}(\omega_0 - \omega)t]\sin[\frac{1}{2}(\omega_0 + \omega)t]. \tag{2.42}$$

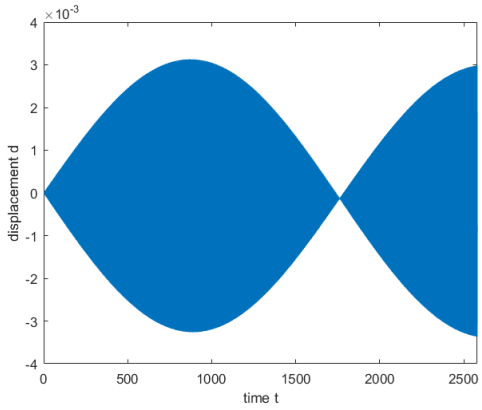

Figure 2.9: Beat pattern at point $(x, y) = (1, 1)$ with forcing frequency $\omega = \sqrt{5}\pi$.

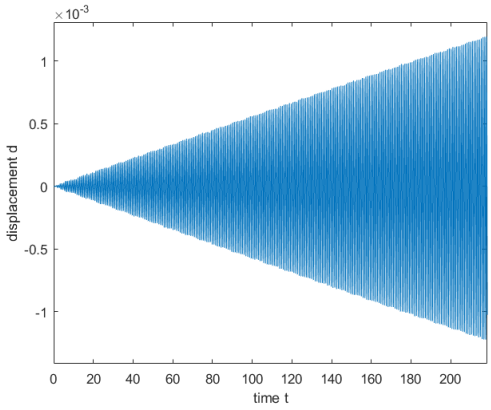

Figure 2.10: A closer look at the beat pattern shown in Fig. 2.9.

In our case, the forcing frequency is given by $\omega = \pi\sqrt{m^2 + s^2}$, which is equal to one of the theoretical resonance frequencies of the wave equation. However, the discretized wave equation given by equation (2.19) actually approximates the equation as follows:

$$u_{tt} + \frac{\Delta t^2}{12}u_{tttt} + O(\Delta t^4) = u_{xx} + \frac{\Delta x^2}{12}u_{xxxx} + O(\Delta x^4) + u_{yy} + \frac{\Delta y^2}{12}u_{yyyy} + O(\Delta y^4). \tag{2.43}$$

If we assume that the fourth order error terms can be ignored, and let

$$u = \cos(\omega_0 t)\cos(m\pi x)\cos(s\pi y),$$

$$h = \Delta x = \Delta y,$$

$$\delta \equiv \frac{h^2}{12},$$

$$\epsilon \equiv \frac{\Delta t^2}{12},$$

and substitute this form for u into equation (2.43), we obtain:

$$\epsilon\omega_0^4 - \omega_0^2 + \pi^2[(m^2 + s^2) - \delta\pi^2(m^4 + s^4)] = 0. \tag{2.44}$$

Then, solving for ω_0^2 yields:

$$\omega_0^2 = \frac{1 \pm \sqrt{1 - 4\epsilon\pi^2[(m^2 + s^2) - \delta\pi^2(m^4 + s^4)]}}{2\epsilon}. \tag{2.45}$$

For small ϵ, we have:

$$\omega_0^2 \approx \frac{1}{2\epsilon}[1 \pm (1 - 2\epsilon\pi^2[(m^2 + s^2) - \delta\pi^2(m^4 + s^4)])]. \tag{2.46}$$

Since ω_0 should approach the value $\pi\sqrt{m^2 + s^2}$ as $\epsilon, \delta \to 0$, we take the root:

$$\omega_0^2 = \pi^2[(m^2 + s^2) - \delta\pi^2(m^4 + s^4)]. \tag{2.47}$$

For small δ, we get:

$$\omega_0 \approx \pi\sqrt{m^2 + s^2} - \frac{\delta\pi^3(m^4 + s^4)}{2\sqrt{m^2 + s^2}}. \tag{2.48}$$

We consider ω_0 as the approximate resonance frequency of the discretized wave equation, which is not exactly equal to the corresponding theoretical resonance frequency of the wave equation.

Now, we can go back to Fig. 2.9 and Fig. 2.10 to check whether the observed periods agree with our theoretical result. From Fig. 2.9 and 2.10, the longer period is $T \approx 3523$ and the shorter period is $T \approx 0.9$.

Since $T = \frac{2\pi}{frequency}$, based on equation (2.42), we know that the longer period should be $|\frac{2\pi}{\frac{1}{2}(\omega_0 - \omega)}|$ and the shorter period should be $\frac{2\pi}{\frac{1}{2}(\omega_0 + \omega)}$. Thus, the longer period should be around 3199 and the shorter period should be about 0.89. Though these results are not exactly the same as the observed values, due to the approximations made, we can conclude that the computed result agrees reasonably well with the theoretical result.

Chapter 3

Elasticity Model

In the previous chapter, we used a wave equation based model to describe the vibrating plate. However, the resulting nodal patterns cannot explain the observed phenomenon very well. For example, for the $(1, 2)$ and $(2, 1)$ modes, the nodal pattern contains an extra square compared to the experimental result. Thus, in this chapter we introduce a more realistic model to describe the vibrating plate based on elasticity theory, which establishes a mathematical model for the deformation of an elastic solid due to the stress, strain and displacement distribution resulting from external forces [14].

3.1 Dimensional and Dimensionless Equations

The elastic force-deformation relations concept was first suggested by Robert Hooke in 1678, but it did not draw a lot of attention for the next 200 years. In the early 19^{th} century, Euler suggested that the elastic force at a point is proportional to the curvature at that point in one dimensional space. Based on this idea, Sophie Germain suggested that in two dimensional space the force of elasticity at a point is proportional to the sum of all the major curvatures at that point. Later on, Lagrange took her assumption and applied the variational method to derive the following equation [7]:

$$\frac{\partial^2 u}{\partial t^2} + k^2 \left(\frac{\partial^4 u}{\partial x^4} + 2\frac{\partial^4 u}{\partial x^2 \partial y^2} + \frac{\partial^4 u}{\partial y^4} \right) = 0, \tag{3.1}$$

where k is a constant, t is time and x, y represent the spatial coordinates. Finally, with many attempts by famous scientists including L. D. Poisson, L. Navier and Gustav R. Kirchhoff, the constant k was determined and equation (3.1) became [2]:

$$\frac{ql^2}{3\rho(1-\mu^2)}\left(\frac{\partial^4 u}{\partial x^4}+2\frac{\partial^4 u}{\partial x^2\partial y^2}+\frac{\partial^4 u}{\partial y^4}\right)+\frac{\partial^2 u}{\partial t^2}=0, \tag{3.2}$$

where q is Young's modulus of elasticity, l is half of the thickness of the plate, ρ is the density of the plate and μ is the ratio of lateral contraction to longitudinal elongation known as Poisson's ratio. Since we are working with square plates, we set the range in space to be $-a \leq x, y \leq a$.

Similar to the wave equation model, we next want to cast equation (3.2) in dimensionless form. We let $\Delta^2 \equiv \left(\frac{\partial^2}{\partial \hat{x}^2}+\frac{\partial^2}{\partial \hat{y}^2}\right)^2 = \frac{\partial^4}{\partial \hat{x}^4}+2\frac{\partial^4}{\partial \hat{x}^2\partial \hat{y}^2}+\frac{\partial^4}{\partial \hat{y}^4}$, the biharmonic operator, $D^2 = \frac{ql^2}{3\rho(1-\mu^2)}$, $(x, y) = (a\hat{x}, a\hat{y})$, $t = \frac{a^2}{D}\hat{t}$, and $u = h(\hat{u})$. Then the non-dimensional equation is written as:

$$\Delta^2 \hat{u}+\frac{\partial^2 \hat{u}}{\partial \hat{t}^2}=0, -1 \leq \hat{x}, \hat{y} \leq 1, \tag{3.3}$$

For simplicity of notation, we will write $\hat{u}$, $\hat{x}$, $\hat{y}$ and $\hat{t}$ as u, x, y and t in the rest of this chapter.

3.2 Boundary Conditions and Analytical solutions

There are various possible boundary conditions associated with the plate problem and each of them would provide different nodal patterns. Table 3.1 shows a list of possible sets of boundary conditions [2].

The first listed set of boundary conditions refers to the plate which has its edges being placed on a handler but not clamped. We call that a simply supported plate. A simply supported plate has zero displacement on the edges but the slope along the edges may vary depending on the loading and the value of Poisson's ratio.

The second set of boundary conditions in the table refers to the situation when the edges of the plate are clamped. Under that situation both the displacement and the slope along the edges of the plate are zero.

The last listed set of boundary conditions describes the case corresponding to our experiment where the plate has free edges. It implies that the displacement along the edges is not fixed and the slope can vary.

Type of Support at Edge $x = a$	Mathematical Expressions
Simple support	$(u)_{x=a} = 0;$ $\left(\frac{\partial^2 u}{\partial x^2} + \mu \frac{\partial u^2}{\partial y^2}\right)_{x=a} = 0$
Fixed edge	$(u)_{x=a} = 0;$ $\left(\frac{\partial u}{\partial x}\right)_{x=a} = 0$
Free-edge	$\left(\frac{\partial^2 u}{\partial x^2} + \mu \frac{\partial u^2}{\partial y^2}\right)_{x=a} = 0;$ $\left[\frac{\partial^3 u}{\partial x^3} + (2-\mu)\frac{\partial^3 u}{\partial x \partial y^2}\right]_{x=a} = 0$

Table 3.1: Different types of boundary conditions.

As stated before, we have the free-edge problem so we are going to apply the third set of listed boundary conditions:

$$\frac{\partial^2 u}{\partial x^2} + \mu \frac{\partial^2 u}{\partial y^2} = 0, \frac{\partial^3 u}{\partial x^3} + (2-\mu)\frac{\partial^3 u}{\partial x \partial y^2} = 0 \text{ along } x = \pm 1, \tag{3.4a}$$

$$\frac{\partial^2 u}{\partial y^2} + \mu \frac{\partial^2 u}{\partial x^2} = 0, \frac{\partial^3 u}{\partial y^3} + (2-\mu)\frac{\partial^3 u}{\partial x^2 \partial y} = 0 \text{ along } y = \pm 1. \tag{3.4b}$$

In addition to the boundary conditions above, we also have extra boundary conditions at the corners:

$$\frac{\partial^2 u}{\partial x \partial y} = 0 \text{ at } (x, y) = (\pm 1, \pm 1), \tag{3.5}$$

which guarantees there is zero torque at the corners.

Note that with these boundary conditions, the solution is not unique. For example, if u_0 is a solution, then so is $u_0 + c_0 + c_1 x + c_2 y$ where c_0, c_1, and c_2 are arbitrary constants. The solution to the wave equation subject to free-edge boundary conditions, on the other hand, is unique to within an additive constant.

To solve equation (3.3), we first assume that the spatial variables x, y and the time

variable t are linearly separable, so we can write the displacement $u(x, y, t)$ as:

$$u(x, y, t) = w(x, y)g(t). \tag{3.6}$$

Since the plate is oscillating over time with a fixed period, we assume the time term $g(t)$ can be written as $A\cos(\omega t - \gamma)$ where A is the amplitude, ω is the frequency and γ is the phase shift. Assuming that $u \propto w(x, y)\cos(\omega t - \gamma)$, then $\Delta^2 w(x, y) = \omega^2 w(x, y)$.

The solution to $(\Delta^2 - \omega^2)w(x, y) = (\Delta - \omega)(\Delta + \omega)w(x, y) = 0$ can be written as $w(x, y) = w_1(x, y) + w_2(x, y)$ where w_1, w_2 satisfy the Helmholtz equations $(\Delta + \omega)w_1 = 0$ and $(\Delta - \omega)w_2 = 0$ [15]. Due to symmetry, we consider oscillations which are symmetrical about the x and y axes, and it follows that $w_1(x, y) \propto \cos(\alpha x)\cos(\beta y)$ and $w_2(x, y) \propto \cosh(\alpha x)\cosh(\beta y)$, where $\omega = \alpha^2 + \beta^2$ and can take on infinitely many possible values. Thus, for a specific value of α, α_m, and β, β_s, the corresponding $w(x, y)$ can be written as $w_{m,s}(x, y)$.

Applying the corner boundary condition (3.5), the solution for $w(x, y)$ then becomes [16]:

$$w(x, y) \equiv w_{m,s}(x, y) \propto \cos(\alpha_m x)\cos(\beta_s y) - A_{m,s}\cosh(\alpha_m x)\cosh(\beta_s y), \tag{3.7}$$

where $A_{m,s} = \frac{\sin(\alpha_m)\sin(\beta_s)}{\sinh(\alpha_m)\sinh(\beta_s)}$. The general solution is then:

$$u(x, y, t) = \sum_{m,s=1}^{\infty} B_{m,s} w_{m,s}(x, y)\cos(\omega_{m,s} t - \gamma), \tag{3.8}$$

where $\omega_{m,s} = \alpha_m^2 + \beta_s^2$. By symmetry and assuming only two modes (m, s) and (s, m) have the same frequency, the nodal lines will satisfy $w_{m,s}(x, y) + w_{s,m}(x, y) = 0$.

Now, how do we compute the values of α_m and β_s? We may substitute the solution:

$$B_{m,s} w_{m,s}(x, y)\cos(\omega_{m,s} t - \gamma),$$

along with the frequency $\omega_{m,s}$, into boundary conditions (3.4) at $x = 1$, to get:

$$\cos(\alpha_m)\cos(\beta_s y) + A_{m,s}\cosh(\alpha_m)\cosh(\beta_s y) = 0, \tag{3.9a}$$
$$\sin(\alpha_m)\cos(\beta_s y) - A_{m,s}\sinh(\alpha_m)\cosh(\beta_s y) = 0. \tag{3.9b}$$

Surprisingly, the above equations do not involve the parameter μ. The study reported in [17] claims that α_m has to satisfy the equation $\sin(\alpha_m)\cosh(\alpha_m) + \cos(\alpha_m)\sinh(\alpha_m) = 0$.

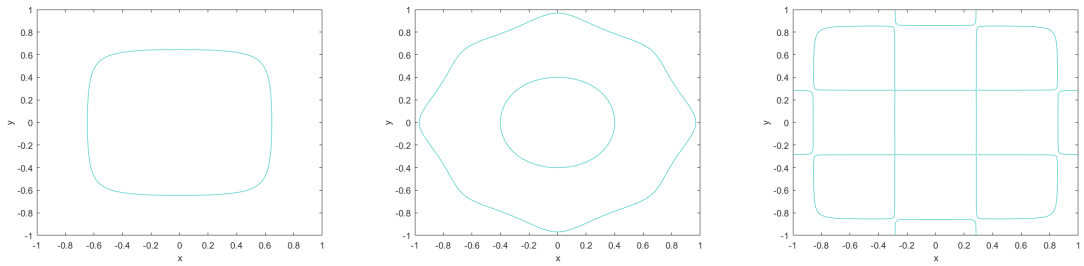

(a) $\alpha \approx 2.3650$, $\beta \approx 2.3650$ (b) $\alpha \approx 2.3650$, $\beta \approx 5.4978$ (c) $\alpha \approx 5.4978$, $\beta \approx 5.4978$

Figure 3.1: Nodal patterns for different modes which are symmetrical to x and y based on elasticity model.

Since the boundary conditions are symmetrical on all edges, it follows that α_m and β_s are both roots of $\chi(\xi) = \sin(\xi)\cosh(\xi) + \cos(\xi)\sinh(\xi) = 0$. The first few roots are $\alpha_1 = \beta_1 = 0$, $\alpha_2 = \beta_2 \approx 2.3650$, $\alpha_3 = \beta_3 \approx 5.4978$, and $\alpha_4 = \beta_4 \approx 8.6394$. Fig. 3.1 shows the corresponding nodal lines for the first three non-trivial modes.

The general solution given by (3.8) is deduced based on the fact that the vibration on the plate with free-edges should result in symmetrical patterns. However, if we ignore the symmetry property, there are four linearly independent solutions to equation (3.3):

$$V_1 = \cos(\alpha x)\cos(\beta y) - C_1\cosh(\alpha x)\cosh(\beta y), C_1 = \frac{\sin\alpha\sin\beta}{\sinh\alpha\sinh\beta}, \tag{3.10a}$$

$$V_2 = \sin(\alpha x)\sin(\beta y) - C_2\sinh(\alpha x)\sinh(\beta y), C_2 = \frac{\cos\alpha\cos\beta}{\cosh\alpha\cosh\beta}, \tag{3.10b}$$

$$V_3 = \cos(\alpha x)\sin(\beta y) - C_3\cosh(\alpha x)\sinh(\beta y), C_3 = \frac{\sin\alpha\cos\beta}{\sinh\alpha\cosh\beta}, \tag{3.10c}$$

$$V_4 = \sin(\alpha x)\cos(\beta y) - C_4\sinh(\alpha x)\cosh(\beta y), C_4 = \frac{\cos\alpha\sin\beta}{\cosh\alpha\sinh\beta}. \tag{3.10d}$$

The α's and β's in each independent solution above satisfy different root equations. The solution can be written as $\hat{A}V_1 + \hat{B}V_2 + \hat{C}V_3 + \hat{D}V_4$ where $\hat{A}$, $\hat{B}$, $\hat{C}$, and $\hat{D}$ are arbitrary constants, and there is no obvious way to determine their values.

We tried to implement the boundary conditions (3.4), but we ran into numerical difficulties. We observed small oscillations forming on the edges after we let the program run for a short period of time. If we run the program for a longer period, we observed large

oscillations at the corners. However, this did not happen when we prescribed the values on the edges. We are still not able to explain this behaviour.

Thus, we considered two different sets of boundary conditions which may be helpful in solving the equation.

The first set of boundary conditions is inspired by the boundary conditions we used for the wave equation, and are given by:

$$\frac{\partial u}{\partial x} = 0, \frac{\partial}{\partial x}(\frac{\partial^2 u}{\partial x^2} + \frac{\partial^2 u}{\partial y^2}) = 0 \text{ along } x = \pm 1, \tag{3.11a}$$

$$\frac{\partial u}{\partial y} = 0, \frac{\partial}{\partial y}(\frac{\partial^2 u}{\partial x^2} + \frac{\partial^2 u}{\partial y^2}) = 0 \text{ along } y = \pm 1. \tag{3.11b}$$

These boundary conditions require that the gradients in u and Δu along the edges are zero. It is easy to show that Δu also satisfies equation (3.3).

Substituting the solution $\cos(\alpha_m x)\cos(\beta_s y) - A_{m,s}\cosh(\alpha_m x)\cosh(\beta_s y)$ into the boundary conditions (3.11), we find that $A_{m,s} = 0$, and thus, $\alpha_m = m\pi$ and $\beta_s = s\pi$, where m and s are integers. Hence, the solution is very similar to that of the wave equation. The only difference lies in the frequency $\omega_{ms} = \alpha_m^2 + \beta_s^2 = \pi^2(m^2 + s^2)$ which is the square of the frequency found for the wave equation. We note that the solution $u(x, y) = \cos(\alpha_m x)\cos(\beta_s y)$ automatically satisfies the corner conditions (3.5).

The second set of boundary conditions is similar to the boundary conditions (3.4), except it does not depend on μ. These boundary conditions are as follows:

$$\frac{\partial^2 u}{\partial x^2} = 0, \frac{\partial}{\partial x}(\frac{\partial^2 u}{\partial x^2} + \frac{\partial^2 u}{\partial y^2}) = 0 \text{ along } x = \pm 1, \tag{3.12a}$$

$$\frac{\partial^2 u}{\partial y^2} = 0, \frac{\partial}{\partial y}(\frac{\partial^2 u}{\partial x^2} + \frac{\partial^2 u}{\partial y^2}) = 0 \text{ along } y = \pm 1, \tag{3.12b}$$

$$\frac{\partial^2 u}{\partial x \partial y} = 0 \text{ along } (x, y) = (\pm 1, \pm 1). \tag{3.12c}$$

Interestingly, if we substitute the symmetrical solution:

$$\cos(\alpha_m x)\cos(\beta_s y) - A_{m,s}\cosh(\alpha_m x)\cosh(\beta_s y),$$

into boundary conditions (3.12), α_m and β_s still satisfy the root equation, $\chi(\xi) = \sin(\xi)\cosh(\xi) + \cos(\xi)\sinh(\xi) = 0$.

If we assume that $\cos(\alpha_m x)\cos(\beta_s y) - A_{m,s}\cosh(\alpha_m x)\cosh(\beta_s y)$ is the solution, by substituting that solution into the boundary conditions, equation (3.12), we get $A_{m,s} = \frac{\sin(\alpha_m)\sin(\beta_s)}{\sinh(\alpha_m)\sinh(\beta_s)}$ which is the same as before. As a result, though the boundary conditions are different from the boundary conditions (3.4), the solution is the same.

Just as we did in Chapter 2, we will also solve the forced elasticity equation given by:

$$\Delta^2 u(x,y,t) + \frac{\partial^2 u}{\partial t^2}(x,y,t) = Q(x,y,t), \tag{3.13}$$

where

$$Q(x,y,t) = \begin{cases} \cos(\omega_{ms} t), & \text{if } x = y = 0 \\ 0, & \text{otherwise} \end{cases}, \tag{3.14}$$

and $\omega_{ms} = \alpha_m^2 + \beta_s^2$.

3.3 Numerical Solution Procedure

In this section, we will discuss how to discretize equation (3.3) so that we can solve it numerically. Again, the explicit method is applied. We let $h = \Delta x = \Delta y$, $n = \frac{2}{h}$. Based on the stability requirement derived in appendix B.1 [18], $\frac{\Delta t}{h^2} \leq \frac{1}{2}$, and so we choose $\Delta t = \frac{h^2}{4}$. We can see that the size of Δt is very restrictive because we are using an explicit method. However, as this equation is linear, we will settle with this scheme.

For $\frac{\partial^2 u}{\partial t^2}$, we discretize it as before:

$$\frac{\partial^2 u}{\partial t^2}(x_i, y_j, t_k) \approx \frac{u_{i,j}^{k-1} - 2u_{i,j}^k + u_{i,j}^{k+1}}{(\Delta t)^2}, \tag{3.15}$$

where k refers to the time step at $t = t_k$, i and j refer to the positions on a uniform spatial grid at $x = x_i$, $y = y_j$.

For the term $\Delta^2 u$, if we apply central differences, it would involve 13 points on the spatial grid at each time step. Instead, we introduce a two-step method here. We let $W \equiv \left(\frac{\partial^2 u}{\partial x^2} + \frac{\partial^2 u}{\partial y^2}\right)$, then equation (3.3) becomes:

$$\left(\frac{\partial^2 W}{\partial x^2} + \frac{\partial^2 W}{\partial y^2}\right) + \frac{\partial^2 u}{\partial t^2} = 0, -1 \leq x, y \leq 1, \tag{3.16}$$

which resembles the two-dimensional wave equation.

Based on the discretization scheme we used for the wave equation given by:

$$\frac{\partial^2 u}{\partial x^2}(x_i, y_j, t_k) \approx \frac{u^k_{i-1,j} - 2u^k_{i,j} + u^k_{i+1,j}}{h^2}, \tag{3.17a}$$

$$\frac{\partial^2 u}{\partial y^2}(x_i, y_j, t_k) \approx \frac{u^k_{i,j-1} - 2u^k_{i,j} + u^k_{i,j+1}}{h^2}, \tag{3.17b}$$

we have:

$$W^k_{i,j} = \frac{u^k_{i-1,j} - 2u^k_{i,j} + u^k_{i+1,j}}{h^2} + \frac{u^k_{i,j-1} - 2u^k_{i,j} + u^k_{i,j+1}}{h^2}, \tag{3.18}$$

where $W^k_{i,j}$ is the numerical approximation to $W(x_i, y_j, t_k)$.

Also,

$$\left(\frac{\partial^2 W}{\partial x^2} + \frac{\partial^2 W}{\partial y^2}\right)(x_i, y_j, t_k) \approx \frac{W^k_{i-1,j} - 2W^k_{i,j} + W^k_{i+1,j}}{h^2} + \frac{W^k_{i,j-1} - 2W^k_{i,j} + W^k_{i,j+1}}{h^2}. \tag{3.19}$$

Applying Boundary Conditions (3.11)

The boundary conditions (3.11) can be written as:

$$\frac{\partial u}{\partial x} = 0, \frac{\partial W}{\partial x} = 0 \text{ along } x = \pm 1, \tag{3.20a}$$

$$\frac{\partial u}{\partial y} = 0, \frac{\partial W}{\partial y} = 0 \text{ along } y = \pm 1. \tag{3.20b}$$

Boundary conditions $\frac{\partial u}{\partial x} = 0$ and $\frac{\partial u}{\partial y} = 0$ are applied when we compute for values of $W^k_{i,j}$ along the corresponding edges. For example, if we suppose $x = 1$ and $y \neq \pm 1$, i.e. $i = n$, $j \neq 0$, and $j \neq n$, we have:

$$W^k_{n,j} = \frac{2u^k_{n-1,j} - 2u^k_{n,j}}{h^2} + \frac{u^k_{n,j-1} - 2u^k_{n,j} + u^k_{n,j+1}}{h^2}, \tag{3.21}$$

where the ghost point $u^k_{n+1,j} = u^k_{n-1,j}$ by central differences.

The second part of the boundary conditions, $\frac{\partial W}{\partial x} = 0$ and $\frac{\partial W}{\partial y} = 0$ along the corresponding edges, is applied when we compute equation (3.19). Again, suppose we have $x = 1$ and $y \neq \pm 1$ ($i = n$ and $0 < j < n$), the ghost point $W^k_{n+1,j} = W^k_{n-1,j}$ by central differences, and equation (3.19) can be written as:

$$\left(\frac{\partial^2 W}{\partial x^2} + \frac{\partial^2 W}{\partial y^2}\right)(x_n, y_j, t_k) \approx \frac{2W^k_{n-1,j} - 2W^k_{n,j}}{h^2} + \frac{W^k_{n,j-1} - 2W^k_{n,j} + W^k_{n,j+1}}{h^2}. \tag{3.22}$$

Applying Boundary Conditions (3.12)

For the second set of boundary conditions, if we replace $\frac{\partial^2 u}{\partial x^2} + \frac{\partial^2 u}{\partial y^2}$ by W, it becomes:

$$\frac{\partial^2 u}{\partial x^2} = 0, \frac{\partial W}{\partial x} = 0 \text{ along } x = \pm 1, \tag{3.23a}$$

$$\frac{\partial^2 u}{\partial y^2} = 0, \frac{\partial W}{\partial y} = 0 \text{ along } y = \pm 1. \tag{3.23b}$$

Again, we apply boundary conditions $\frac{\partial^2 u}{\partial x^2} = 0$ and $\frac{\partial^2 u}{\partial y^2} = 0$ for computing the values of $W^k_{i,j}$ along the corresponding edges. For example, when $x = 1$ and $y \neq \pm 1$, i.e. $i = n$, $j \neq 0$ and $j \neq n$, from the boundary condition $\frac{u^k_{n+1,j} - 2u^k_{n,j} + u^k_{n-1,j}}{h^2} \approx \frac{\partial^2 u}{\partial x^2}(x_n, y_j, t_k) = 0$ we have:

$$W^k_{n,j} = \frac{u^k_{n,j+1} - 2u^k_{n,j} + u^k_{n,j-1}}{h^2}. \tag{3.24}$$

Since the second part of the boundary conditions are same as the boundary conditions in equation (3.11), we apply them the same way as given by equation (3.22).

3.4 Results and Analysis

In this section results based on different sets of boundary conditions are discussed.

Boundary Conditions Derived from the Wave Equation

For the set of boundary conditions (3.11), as we have an analytical solution, we will first check our numerical scheme by setting an initial displacement with zero velocity:

$$u(x, y, 0) = U_0(x, y), \tag{3.25a}$$

$$\frac{\partial u}{\partial t}(x, y, 0) = 0. \tag{3.25b}$$

Then we will force the plate at the theoretical resonance frequency with zero initial displacement and velocity:

$$u(x, y, 0) = 0, \tag{3.26a}$$

$$\frac{\partial u}{\partial t}(x, y, 0) = 0. \tag{3.26b}$$

First, we let $u(x, y, 0) = U_0(x, y)$, where

$$U_0(x, y) = \cos(m\pi x)\cos(s\pi y) + \cos(s\pi x)\cos(m\pi y),$$

m and s are both non-negative integers. To be consistent, we will still test the (1,2) and (2,1) modes as we did for the wave equation. The resulting nodal pattern should be exactly the same as the nodal pattern we have in Fig. 2.1. Other settings are as following: $h = \Delta x = \Delta y = 0.02$, $\Delta t = \frac{h^2}{4} = 0.0001$ and $T = 10$.

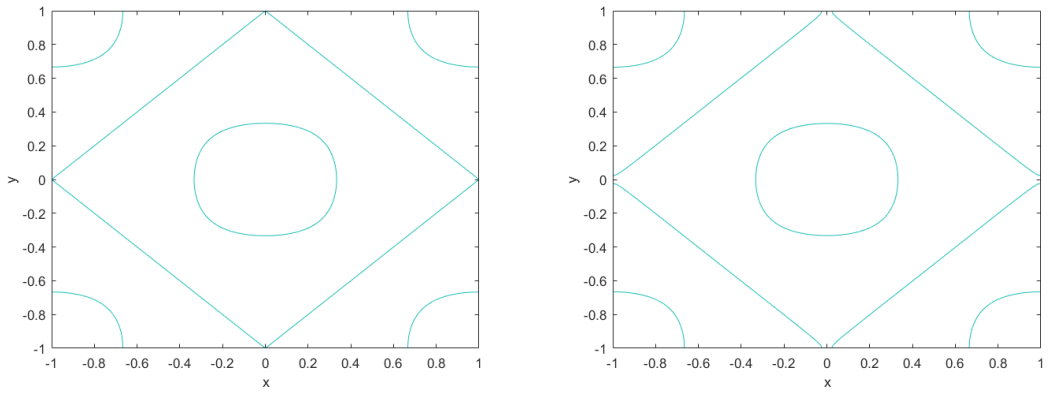

(a) The nodal pattern at $t = 0$.

(b) The nodal pattern at $t = 10$.

Figure 3.2: The nodal patterns under the boundary conditions (3.11) with frequency $\omega = \pi^2 + 4\pi^2$.

Grid size h	Error	Ratio
0.1	0.065527	-
0.05	0.01528	4.2893
0.025	0.00370	4.1245
0.0125	0.000913	4.0562
0.00625	0.00023	4.0226
0.003125	0.00006	4.0129

Table 3.2: The errors and the ratio between errors.

Fig. 3.2 shows the nodal patterns at $t = 0$ and $t = 10$. Indeed, the nodal pattern did not change during this time range, as we observed with the wave equation. Table 3.2 shows the error computed according to equation (2.36) when the stopping time T was 0.05. We

can see that the ratio of consecutive errors converges to 4 as the grid size h is reduced by a factor of 2 at each time as expected.

We next forced the elaticity equation with the same frequency $\omega = 5\pi^2$ to check whether the nodal pattern shown in in Fig. 3.2 would eventually appear.

Fig. 3.3 shows the nodal pattern at $t = 60$ and the displacement at the corner (1,1) during this period of time. The nodal pattern at $t = 60$ is very similar to that in Fig. 3.2. On the right hand side of Fig. 3.3, we see beats as we did with the wave equation. From this it appears that the numerical scheme seems to be working correctly.

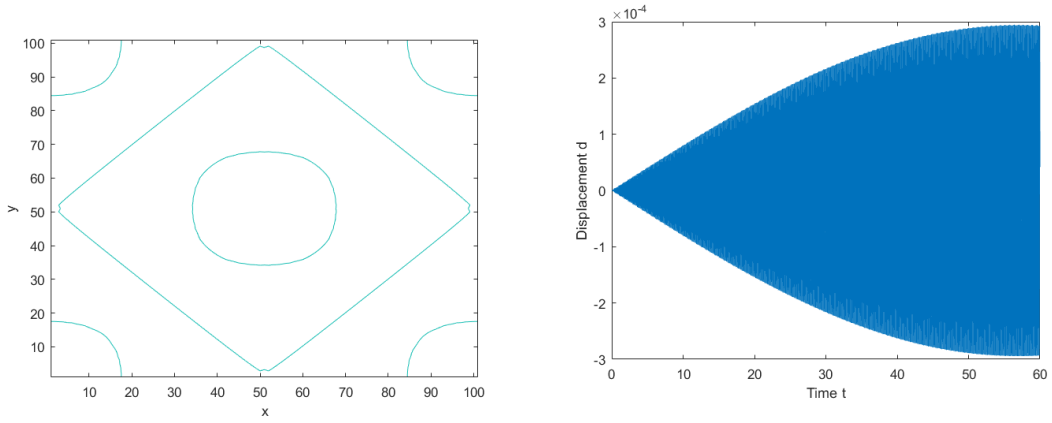

(a) The nodal pattern at $t = 60$.

(b) The displacement of corner point (1,1) versus time.

Figure 3.3: The forced elasticity equation with boundary conditions (3.11).

Boundary Conditions (3.12)

We will assume that the resonance frequency is given by $\alpha_m^2 + \beta_s^2$, where both α_m and β_s are the roots of the equation $\chi(\xi) = \sin(\xi)\cosh(\xi) + \cos(\xi)\sinh(\xi)$. The first three roots are 0, 2.3650, and 5.4978.

Again, we let $h = \Delta x = \Delta y = 0.02$, $\Delta t = \frac{h^2}{4} = 0.0001$, and the final time $T = 60$. We initialize the plate to be at rest with zero velocity at time $t = 0$. According to equation (3.13), we will force the plate at the centre using four different frequencies shown in Table 3.3, and compare the resulting nodal patterns. Figs. 3.4, 3.6, 3.7 and 3.8 show the nodal patterns at the final time $T = 60$ and the displacement of the corner (1,1) over time.

α	β	Forcing Frequency $(\alpha^2 + \beta^2)$
0	2.3650	5.5933
2.3650	2.3650	11.1866
2.3650	5.4978	35.8192
5.4978	5.4978	60.4517

Table 3.3: Frequencies and corresponding α's and β's.

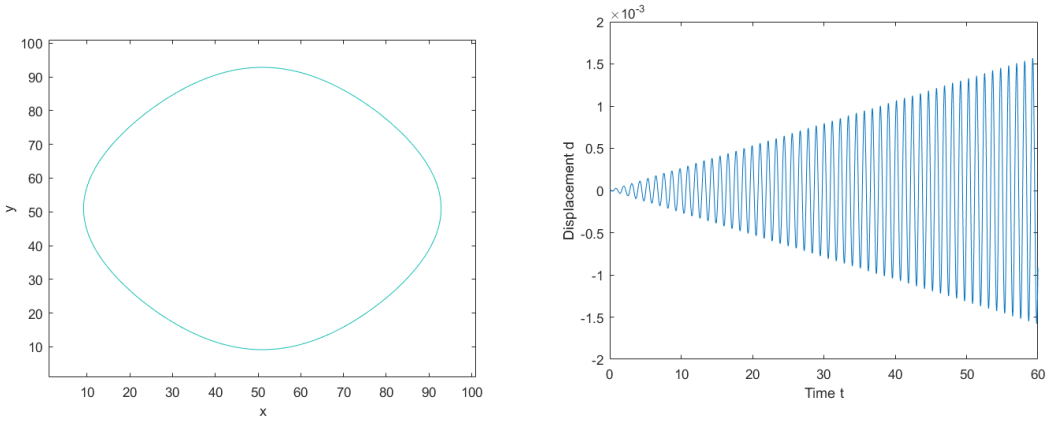

(a) The nodal pattern at $t = 60$.

(b) The displacement of corner point (1,1) over time.

Figure 3.4: The forced elasticity model with forcing frequency $\omega = 5.5933$.

According to Fig. 3.4, which corresponds to the lowest non-zero forcing frequency, we don't see an obvious beat pattern as the amplitude keeps increasing over time. Fig. 3.5 shows the displacement of corner (1,1) over a longer time interval $T = 2000$ and we now see beats. This suggests that the forcing frequency is very close to the resonance frequency. The nodal pattern in Fig. 3.4, was observed to remain the same with time.

In both Fig. 3.6 and Fig. 3.7, the displacement of the corner (1,1) show beats, which suggests that the forcing frequencies are slightly different from the resonance frequencies. Also, we note that when forcing frequency $\omega = 11.1866$, the resulting nodal pattern is similar to the observed experimental result for frequency 190 Hz as shown in Fig. 1.7.

In Fig. 3.8, which shows the result when the plate is forced at frequency $\omega = 60.4517$, the nodal pattern is not as stable as with the lower frequencies. That is, the pattern changes over a time interval and keeps repeating. The displacement of the corner (1,1) also show less obvious beats. This indicates that either the forcing frequency is not close

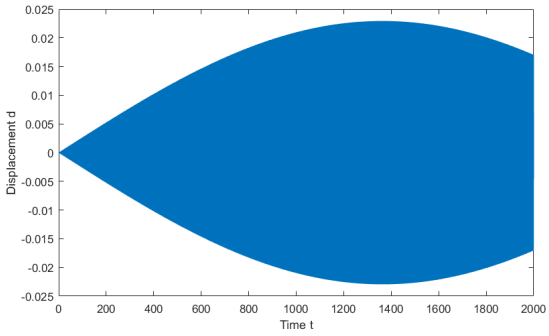

Figure 3.5: The displacement of corner point (1,1) up to time T = 2000 with forcing frequency $\omega = 5.5933$.

enough to any resonance frequency, or there are multiple sets of possible nodal patterns co-existing on the plate, so that the displacement of the corner is irregular.

Now, let us take a closer look at the case with forcing frequency $\omega = 35.8192$, which corresponds to the (1,2) and (2,1) modes. Fig. 3.9 shows the nodal patterns at different times. If we go back to Fig. 3.7, we can see that the beats have a long period $T \approx 11.7600$ and a short period $T \approx 0.1739$. As we know the forcing frequency ω, we can compute the resonance frequency ω_0 by assuming that the two equations from section 2.7 apply:

$$\frac{2\pi}{\frac{1}{2}(\omega_0 - \omega)} = 11.7600, \tag{3.27a}$$

$$\frac{2\pi}{\frac{1}{2}(\omega_0 + \omega)} = 0.1739. \tag{3.27b}$$

By substituting $\omega = 35.8192$ into the two equations in (3.27), we get $\omega_0 \approx 36.4375$ and $\omega_0 \approx 36.8877$. By taking the average, we can force the plate with frequency $\omega = 36.6626$, and compare the nodal pattern. Fig. 3.10 shows the shapes of the nodal patterns at different times with this forcing frequency. Comparing Fig. 3.9 and Fig. 3.10, we can see that the nodal pattern is more stable now. The displacement of the corner (1,1) at this new forcing frequency is shown in Fig. 3.11 and we can see that beats still exist but with a much longer period. This implies that the new forcing frequency is much closer to the resonance frequency. We can repeat this procedure iteratively to obtain a more accurate estimate of the resonance frequency.

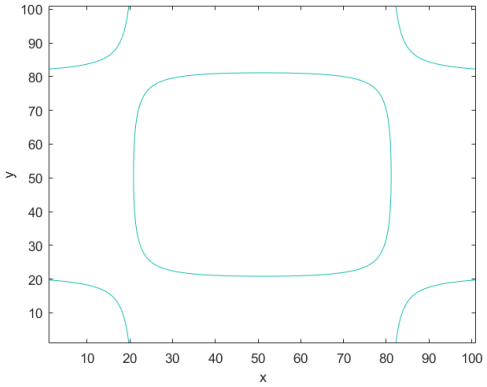

(a) The nodal pattern at $t = 60$.

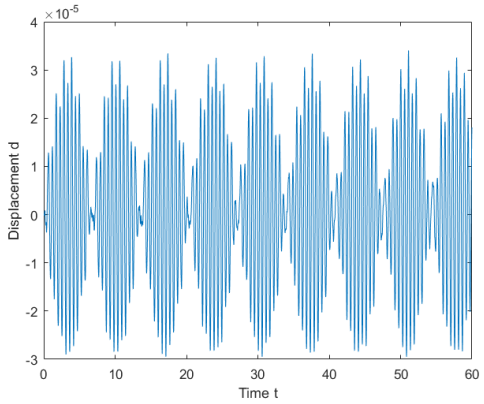

(b) The displacement of corner point (1,1) over time.

Figure 3.6: The forced elasticity model with forcing frequency $\omega = 11.1866$.

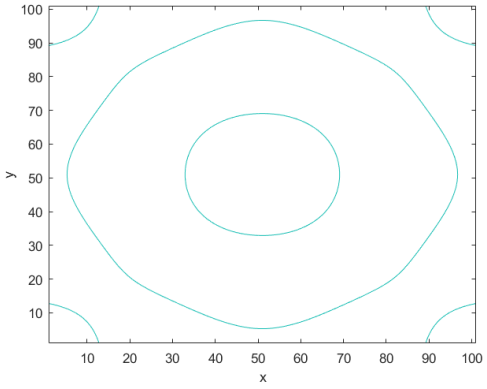

(a) The nodal pattern at $t = 60$.

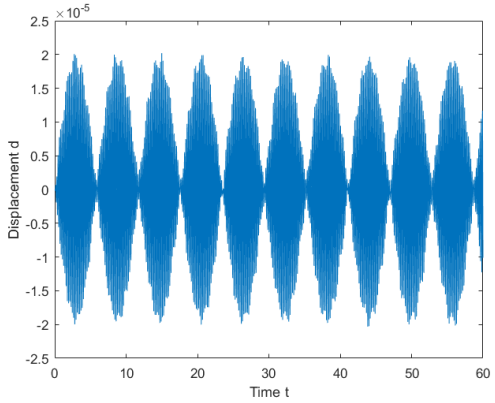

(b) The displacement of corner point (1,1) over time.

Figure 3.7: The forced elasticity model with forcing frequency $\omega = 35.8192$.

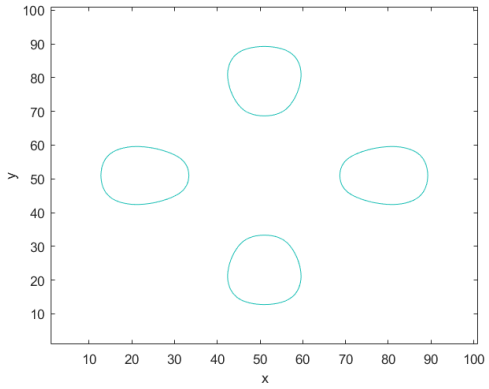

(a) The nodal pattern at $t = 60$.

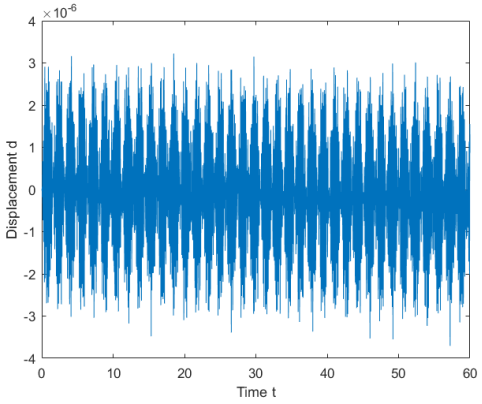

(b) The displacement of corner point (1,1) over time.

Figure 3.8: The forced elasticity model with forcing frequency $\omega = 60.4517$.

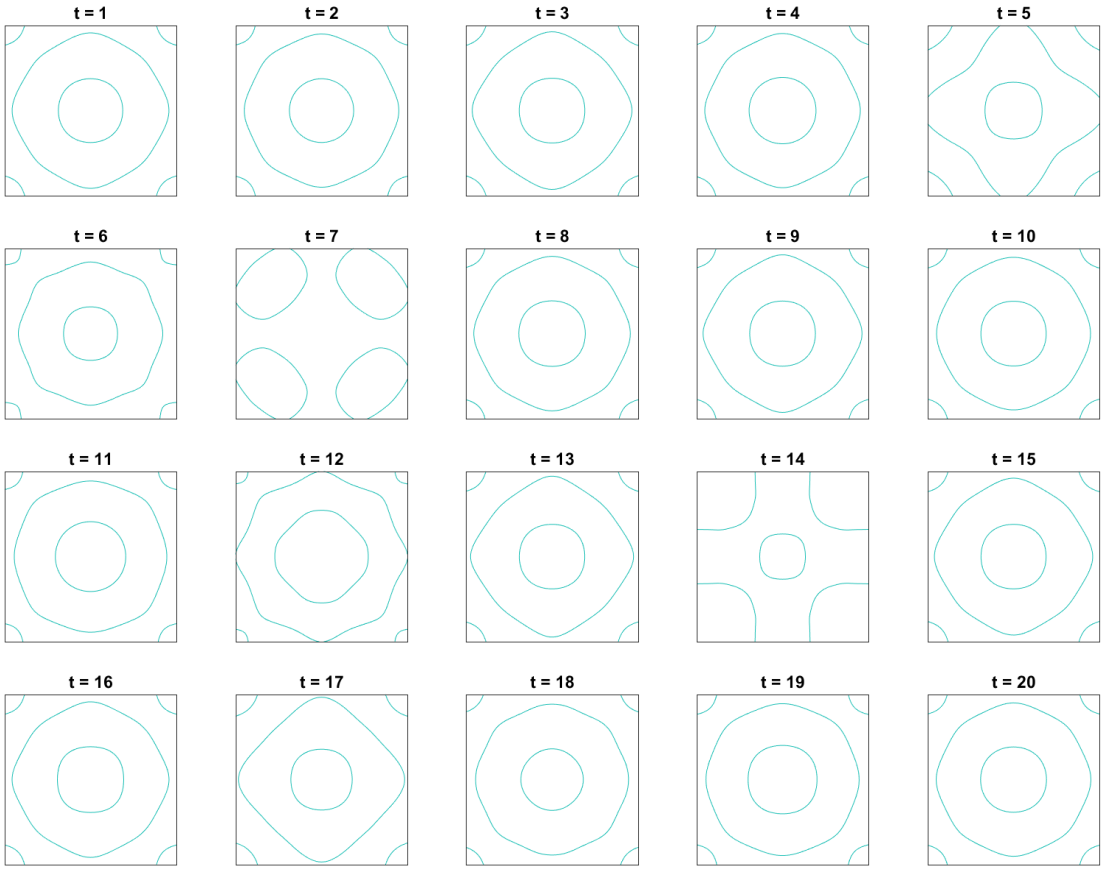

Figure 3.9: The forced elasticity model with forcing frequency $\omega = 35.8192$.

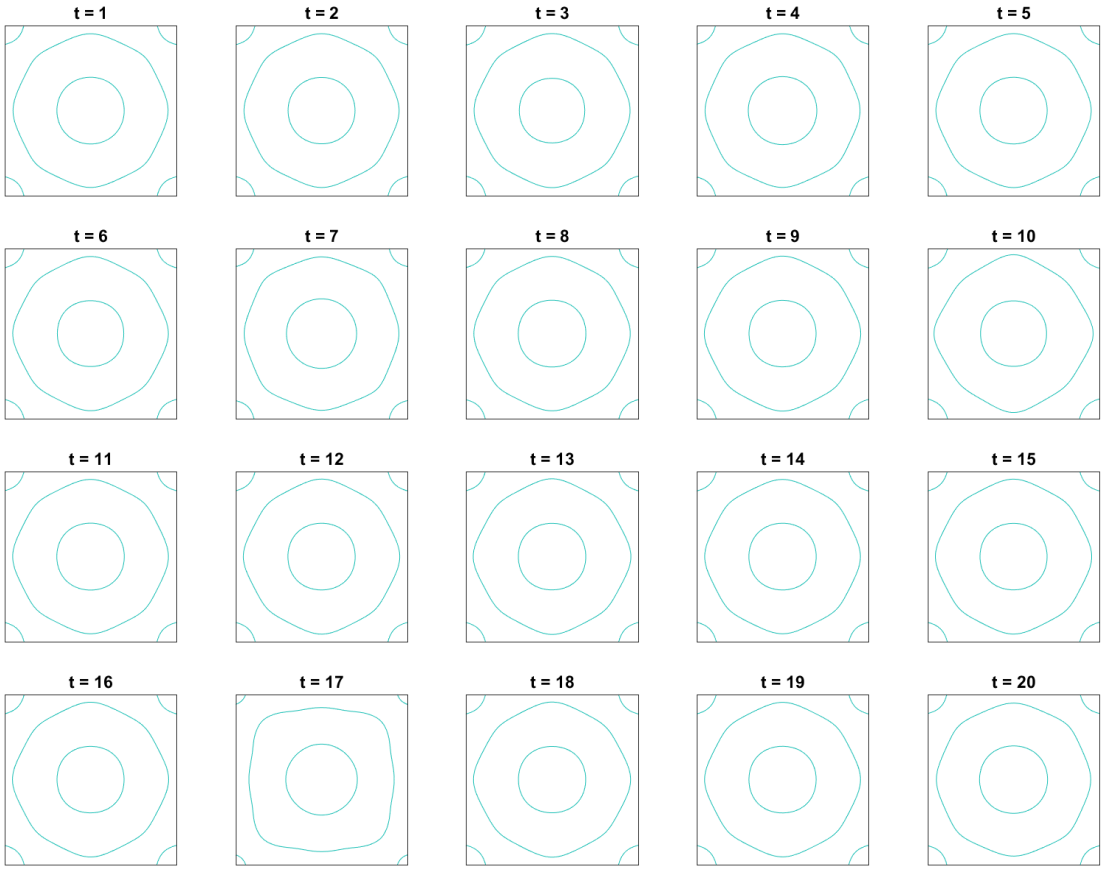

Figure 3.10: The forced elasticity model with forcing frequency $\omega = 36.6625$.

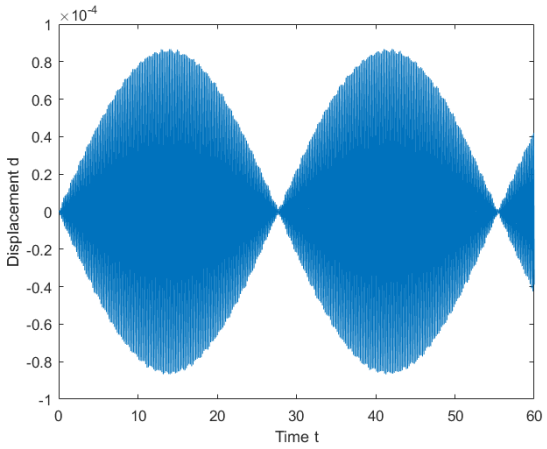

Figure 3.11: The displacement of the corner (1,1) with a forcing frequency of $\omega = 36.6625$.

Chapter 4

Conclusion

Here we briefly summarize this research in two sections. We will first discuss various challenges we have encountered. Then we will discuss possible directions of future work.

4.1 Challenges

In this report we have used two different models, the wave equation model and the model based on elasticity theory. The wave equation model can only be applied to infinitesimally thin and infinitely flexible membranes. Thus, though we can get stable nodal patterns, the numerical result cannot reproduce the phenomenon we observed in the experiments.

An issue regarding the eigenvalue/eigenvector approach in section 2.7 is as follows. Though we figured out a way to generate the nodal pattern based on eigenvectors, we still have to distinguish the fixed centre and free centre modes by examining the eigenvalues, which is not always possible. Based on the general solution, there should be a principle that indicates which eigenvalues are associated with certain frequencies corresponding to fixed and free centres.

For the elasticity model, though it is closer to the real situation, with the free-edge boundary conditions, it is much more difficult to solve. When we cast the elasticity equation (3.2) in dimensionless form, the general solution does not involve the plate properties, yet the free-edge boundary conditions still rely on the Poisson's ratio.

In addition, if we apply the free-edge boundary conditions, by setting $\mu = 1$, and force the plate at the centre according to equation (3.13), the four corners of the plate never

oscillate, which implies that it shares the same nodal pattern as if we clamped all four corners of the plate.

Another issue we encountered is that as the forcing frequency becomes higher, it is harder to find the corresponding resonance frequency by observing beats. The first reason is that it is possible to have more modes co-existing on the plate as the forcing frequency gets larger. In addition, the differences between the theoretical resonance frequencies and the resonance frequencies corresponding to the numerical scheme increases. For the finite difference scheme used for the wave equation, we found that the resonance frequency is approximated by equation (2.48), where it has a term added to the theoretical value. As frequency gets larger, the value of the term also gets larger. We believe that a similar situation happens with the finite difference scheme for the elasticity equation. Thus, simply looking at the displacement of one point over time to determine the resonance frequency becomes very difficult with higher forcing frequencies.

4.2 Future Work

Besides the improvements related to the issues and challenges discussed in the previous section, there are other possibilities for future work.

The first one is to apply the eigenvalue/eigenvector approach to the elasticity equation as we did for the wave equation. We figured out that for each pair of eigenvectors associated with the same eigenvalues, adding them to their transposes resulted in better agreement with the theoretical nodal patterns. Since the elasticity equation is a linear partial differential equation, it is possible to express the finite difference equation as an eigenvalue equation. Then, we can reproduce the nodal patterns as we did for the wave equation. In addition, all the associated eigenvalues which correspond to the square of the resonance frequencies can be found.

In chapter 3, the explicit finite difference scheme requires the time step size, $\Delta t \leq \frac{h^2}{2}$, which is very restrictive. Thus, we can update the finite difference scheme using an implicit method to save time.

Another direction for future work is to update the simulation so that it is closer to the experiment. In the physical experiment, we are using a wave generator to vibrate the steel plate at the centre with a constant amplitude. However, in our simulations, the amplitude of the centre of the plate is never constant. The external force term should be correlated to the vertical displacement of the centre of the plate, so that the amplitude remains constant.

Lastly, more work can be done to determine the exact analytical solution to the elasticity equation with the free-edge boundary conditions. As noted in section 3.2, it is not clear that the solutions for α and β reported in [17] are correct.

APPENDICES

Appendix A

Matlab Codes

A.1 Wave Equation With Initial Displacement

Here is a sample Matlab code for numerically computing the displacement of plate and nodal lines at time $T = 10$, with initial displacement equal to a standing wave, based on wave equation.

```
n = 100; % number of intervals
x = linspace(-1,1,n+1); % mesh grid in x direction
y = linspace(-1,1,n+1); % mesh grid in y direction
h = 2/n;
m = 2; % The first integer (m)
mm =1; % The second integer (n)
dt = h/2; %\Delta t
T = 10; % The stopping time
Uo = cos(m*pi*x)'*cos(mm*pi*y)+cos(mm*pi*x)'*cos(m*pi*y); % Time step = k-1
Uoo = cos(m*pi*x)'*cos(mm*pi*y)+cos(mm*pi*x)'*cos(m*pi*y); % Time step = k-2
U = zeros(n+1);
for t=1:T/dt
    for i = 1:n+1
        for j = 1:n+1
            % applying boundary conditions by central difference
            % method
            if i == 1
```

```
            i_1 = 2;
        else
            i_1 = i-1;
        end
        if j == 1
            j_1 = 2;
        else
            j_1 = j-1;
        end
        if i == n+1
            i1 = n;
        else
            i1 = i+1;
        end
        if j == n+1
            j1 = n;
        else
            j1 = j+1;
        end
        U(i,j) = (Uo(i_1,j)-4*Uo(i,j)+Uo(i1,j)+Uo(i,j_1)+Uo(i,j1))
                 /h^2*dt^2-Uoo(i,j)+2*Uo(i,j);
    end
end
    Uoo = Uo; % Update the previous time steps
    Uo = U;
end
    figure(1)
    surf(x,y,U);
    figure(2)
    contour(x,y,U,[0 0]);
```

A.2 Forced Wave Equation

Here is a sample Matlab code for numerically computing the displacement of plate and nodal lines at time $T = 100$, with initial vertical displacement of the plate equal to 0, based on periodically forced wave equation.

```
n = 100; %number of intervals on each axis
x = linspace(-1,1,n+1);
y = linspace(-1,1,n+1);
alpha = 5;
force = @(eps,w,t) alpha*cos(w*t);
h = 2/n;
dt = h/2;
m = 1;
mm = 2;
T = 100;
w = pi*sqrt(1^2 + 2^2);
Uo = zeros(n+1);
Uoo = Uo;
for t=1:T/dt
    for i = 1:n+1
        for j = 1:n+1
            if ~((i == (n+2)/2) && (j == (n+2)/2))
                if i == 1
                    i_1 = 2;
                else
                    i_1 = i-1;
                end
                if j == 1
                    j_1 = 2;
                else
                    j_1 = j-1;
                end
                if i == n+1
                    i1 = n;
                else
                    i1 = i+1;
                end
                if j == n+1
                    j1 = n;
                else
                    j1 = j+1;
                end
                U(i,j) = (Uo(i_1,j) - 4*Uo(i,j) + Uo(i1,j) + Uo(i,j_1) + Uo(i,j1))
```

```
                        /h^2*dt^2 - Uoo(i,j) + 2*Uo(i,j);
            end
        end
    end
    kk = (n+2)/2;
    U(kk,kk) = ((Uo(kk-1,kk) - 4*Uo(kk,kk) + Uo(kk+1,kk) + Uo(kk,kk-1) +
              Uo(kk,kk+1))/h^2 + force(alpha,w,dt*(t - 1)))*dt^2 - Uoo(kk,kk) +
              2*Uo(kk,kk);
    Uoo = Uo;
    Uo = U;
    if mod(t,10)==0
        figure(1)
        surf(x,y,U);
        figure(2)
        contour(U,[0 0]);
        pause(0.05)
    end
end
```

Appendix B

Other Computations

B.1 Stability Region for Elasticity Model in One Dimensional Space

In this section, we will determine the stability region for the one dimensional elasticity equation.

Consider the partial differential equation: $\frac{\partial^2 u}{\partial t^2} + \frac{\partial^4 u}{\partial x^4} = 0$. In discretized form, denoting $U_i^k \equiv u(x_i, t_k)$, we can write it as:

$$\frac{U_i^{k+1} - 2U_i^k + U_i^{k-1}}{(\Delta t)^2} + \frac{U_{i+2}^k - 4U_{i+1}^k + 6U_i^k - 4U_{i-1}^k + U_{i-2}^k}{(\Delta x)^4} = 0, \tag{B.1}$$

which has truncation error $O([\Delta t]^2 + [\Delta x]^2)$. Rearranged equation (B.1) gives:

$$U_i^{k+1} = 2(1 - 3\lambda)U_i^k - \lambda(U_{i+2}^k - 4U_{i+1}^k - 4U_{i-1}^k + U_{i-2}^k) - U_i^{k-1}, \tag{B.2}$$

where $\lambda = \frac{(\Delta t)^2}{(\Delta x)^4}$.

If we set $u(x,t) = Re(\mathrm{e}^{j\alpha x - \omega t})$, where $j \equiv \sqrt{-1}$, then:

$$\begin{aligned}
&\frac{\partial^2 u}{\partial t^2} + \frac{\partial^4 u}{\partial x^4} \\
&\approx u\left[\frac{\mathrm{e}^{-\omega\Delta t} - 2 + \mathrm{e}^{\omega\Delta t}}{(\Delta t)^2} + \frac{\mathrm{e}^{2j\alpha\Delta x} - 4\mathrm{e}^{j\alpha\Delta x} + 6 - 4\mathrm{e}^{-j\alpha\Delta x} + \mathrm{e}^{-2j\alpha\Delta x}}{(\Delta x)^4}\right] \\
&= \frac{u}{(\Delta t)^2}[2\cosh(\omega\Delta t) - 2 + \lambda(2\cos(2\alpha\Delta x) - 8\cos(\alpha\Delta x) + 6)] \\
&= \frac{2u}{(\Delta t)^2}[\cosh(\omega\Delta t) - (1 - 3\lambda) + \lambda(\cos(2\alpha\Delta x) - 4\cos(\alpha\Delta x))].
\end{aligned} \tag{B.3}$$

For $u(x,t)$ to satisfy the equation, $\frac{\partial^2 u}{\partial t^2} + \frac{\partial^4 u}{\partial x^4} = 0$, the following relation must be true:

$$\cosh(\omega\Delta t) = (1 - 3\lambda) - \lambda(\cos(2\alpha\Delta x) - 4\cos(\alpha\Delta x)), \tag{B.4}$$

or:

$$\mathrm{e}^{-2\omega\Delta t} - [2(1 - 3\lambda) - \lambda(\cos(2\alpha\Delta x) - 4\cos(\alpha\Delta x))]\mathrm{e}^{-\omega\Delta t} + 1 = 0. \tag{B.5}$$

By solving the equation above, we get:

$$\begin{aligned}
\mathrm{e}^{-\omega\Delta t} = (1 - 3\lambda) - \lambda(\cos(2\alpha\Delta\omega) - 4\cos(\alpha\Delta x)) \pm \\
\sqrt{((1 - 3\lambda) - \lambda(\cos(2\alpha\Delta\omega) - 4\cos(\alpha\Delta x)))^2 - 1}.
\end{aligned} \tag{B.6}$$

Note that we have $u(x,t) = \cos(\alpha x)\mathrm{e}^{-\omega t} = \cos(\alpha x)(\mathrm{e}^{-\omega\Delta t})^{\frac{t}{\Delta t}}$, so $u(x,t)$ satisfies:

$$u(x,t) = \cos(\alpha x)[a \pm \sqrt{a^2 - 1}]^{\frac{t}{\Delta t}}, \tag{B.7}$$

where:

$$\begin{aligned}
a &= (1 - 3\lambda) - \lambda(\cos(2\alpha\Delta x) - 4\cos(\alpha\Delta x)) \\
&= (1 - 3\lambda) + \lambda(3 - 2[\cos(\alpha\Delta x) - 1]^2) \\
&= 1 - 2\lambda[\cos(\alpha\Delta x) - 1]^2.
\end{aligned} \tag{B.8}$$

In order to guarantee that the solution $u(x,t)$ remains bounded as $t \to \infty$, we need that:

$$-1 \leq a \pm \sqrt{a^2 - 1} \leq 1. \tag{B.9}$$

To satisfy this, we require that $-1 \leq a \leq 1$, because if we let $z \equiv a \pm \sqrt{a^2 - 1} = a \pm j\sqrt{1 - a^2}$, we have:

$$zz^* = (a \pm j\sqrt{1 - a^2})(a \mp j\sqrt{1 - a^2}) = a^2 + (1 - a^2) = 1. \tag{B.10}$$

Then:

$$\begin{aligned} &-1 \leq a \leq 1 \\ &-1 \leq 1 - 2\lambda[\cos(\alpha\Delta x) - 1]^2 \leq 1 \\ &-2 \leq -2\lambda[\cos(\alpha\Delta x) - 1]^2 \leq 0. \end{aligned} \tag{B.11}$$

By taking the maximum value of $[\cos(\alpha\Delta x) - 1]^2$, we get:

$$-2 \leq -8\lambda \leq 0. \tag{B.12}$$

Hence, $0 \leq \frac{(\Delta t)^2}{(\Delta x)^4} = \lambda \leq \frac{1}{4}$. The stability region for the one dimensional elasticity model is then $\frac{\Delta t}{(\Delta x)^2} \leq \frac{1}{2}$, which is consistent and in exact agreement with the convergence criteria for the heat equation $\frac{\partial u}{\partial t} = \frac{\partial^2 u}{\partial x^2}$.

References

[1] Gerhard Wanner Martin J. Gander. From Euler, Ritz, and Galerkin to modern computing. *SIAM REVIEW*, 54, 2012.

[2] R. Szilard. *Theories and Applications of Plate Analysis: Classical, Numerical and Engineering Methods*. John Wiley & Sons, Inc, 2004.

[3] Ernst Chladni - Chladni figures (Klangfiguren). https://monoskop.org/Ernst_Chladni#Chladni_figures_.28Klangfiguren.29.

[4] University of Oklahoma, Dept. of Physics and Astronomy. *Chladni Patterns*, 2002. https://www.nhn.ou.edu/~johnson/Education/Juniorlab/Chladni/2002-Chladni_S2002.pdf.

[5] S.M. Lehar. Directional harmonic theory: A computational gestalt model to account for illusory contour and vertex formation. *Perception*, 32:423–48, 2003.

[6] H.-J. Stockmann. *Chladni meets Napoleon*. Eur. Phys. J., 2007.

[7] A.M. Hill. Sophie germain: A mathematical biography. Master's thesis, University of Oregon, Eugene, Oregon, 1995.

[8] Emmanuel DiBenedetto. *Partial Differential Equations*. Birkhuser Boston, 2010.

[9] Daniel A. Russell. *Acoustics and Vibration Animations*. Pennsylvania State University, 1996. https://www.acs.psu.edu/drussell/Demos/superposition/superposition.html.

[10] Artur B. Adib. *Study Notes on Numerical Solutions of the Wave Equation with the Finite Difference Method*. Universidade Federal do Ceará, Brazil, 2000. https://arxiv.org/pdf/physics/0009068.pdf.

[11] Richard Haberman. *Elementary applied partial differential equations : with Fourier series and boundary value problems*. Upper Saddle River, NJ : Prentice Hall, 1998.

[12] World Heritage Encyclopedia. *Beat (acoustics)*. Project Gutenberg Self-Publishing Press.

[13] NayerEradat. *Chapter 5 Superposition of Waves*. Erbion Consultants, 2009.

[14] Martin H. Sadd. *Elasticity - Theory, Applications, and Numerics (2nd Edition)*. Elsevier, 2009.

[15] Michael P. Lamoureux. *The mathematics of PDEs and the wave equation*. University of Calgary, August 2006.

[16] V.E. Nazaokinskii A.D. Polyanin. *Handbook of Linear Partial Dierential Equations for Engineers and Scientists, 2nd Ed.* CRC Press, New York, 2016.

[17] S.V. Bosakov. Eigenfrequencies and modied eigenmodes of a rectangular plate with free edges. *Journal of Applied Mathematics and Mechanics*, 2008.

[18] H. B. Keller E. Isaacson. *Analysis of Numerical Methods*, page 501. John Wiley & Sons, Inc., 1966.